SOURCES OF SEISMIC NOISE

IN

BOREHOLES

by

Wafik Bulind Beydoun

M. S. T. Géophysique-Géotechnique
Université Pierre et Marie Curie
Paris, France
(1980)

SUBMITTED TO THE DEPARTMENT OF
EARTH AND PLANETARY SCIENCES
IN PARTIAL FULFILLMENT
OF THE REQUIREMENTS
FOR THE DEGREE OF

MASTER OF SCIENCE

at the

MASSACHUSETTS INSTITUTE OF TECHNOLOGY

June 1982

Signature of Author _____

Department of Earth and Planetary Sciences
May 18, 1982

Certified by _____

M. Nafi Toksöz
Thesis Supervisor

Accepted by _____

Theodore R. Madden
Chairman, Department Committee

SOURCES OF SEISMIC NOISE

IN BOREHOLES

by

Wafik Bulind Beydoun

Submitted to the Department of Earth and Planetary Sciences on May 18, 1982 in partial fulfillment of the requirements for the Degree of Master of Science

ABSTRACT

The first part of this thesis is concerned with the coupling of a seismic tool with the formation in a borehole. Two resonance models are presented and the transfer function of the coupling evaluated. The resonance frequency can be controlled and shifted away from the VSP frequency bandwidth. The key parameters are the tool's mass, the clamping and the surface of contact of the tool with the formation.

In the second part, the generation of tube waves due to the closure of a fluid-filled fracture intersecting the borehole is investigated. This phenomenon occurs when an incident P-wave impinges on the fracture. From the tube wave amplitude normalized to the P-wave amplitude in the formation, we can estimate the in-situ fracture width.

Thesis Supervisor: M. Nafi Toksoz

Title: Professor of Geophysics

ACKNOWLEDGEMENT

I am indebted to my advisor, Nafi Toksöz, who first aroused my interest in borehole studies. His ideas and comments both clarified my thinking and improved this manuscript.

Discussions with Drs. Arthur Cheng and Joseph Walsh were very constructive. The first part of this thesis was initiated at Schlumberger in Clamart during the summer of 1981. I wish to thank M. Bruno Seeman for letting me use the available data. Dorothy Frank typed the major part of this thesis with incredible skill and speed.

Contents

Sections Page

Part I

SEISMIC TOOL-FORMATION COUPLING IN BOREHOLES

List of symbols

ω = Angular frequency

V_p, V_s = Compressional and shear wave velocity, respectively

$k_\alpha = \omega/V_p$ Compressional wave number

$k_\beta = \omega/V_s$ Shear wave number

$$\gamma^2 = \frac{V_p^2}{V_s^2} = k_\beta^2/k_\alpha^2 > 1$$

$I(\omega)$ = Dynamic radiation compliance

$T(\omega)$ = Coupling transfer function

M = Tool's mass

$DD = 2d$ Length of contact of the tool in the z direction

δ = Width of contact surface of tool

w = Vertical displacement

λ, μ = Lame's elastic constants

ν, ρ = Poisson's ratio and mean density, respectively

$H_n(z) \equiv H_n^{(1)}(\xi)$ n-th order Hankel function of the first kind

$H_n'(\xi)$ and $H_n''(\xi)$ are the first and second derivatives with respect to ξ of $H_n(\xi)$.

$\dot{w}$ and $\ddot{w}$ denotes the first and second derivatives, respectively of the function w with respect to the time variable t.

ξ = axial (vertical) wave number

$h = (k_\alpha^2 - \xi^2)^{1/2}$ horizontal P wave number (Axicylin)

$k = (k_\beta^2 - \xi^2)^{1/2}$ horizontal S wave number (Axicylin)

$\in$ means 'belongs to'

$\forall$ means 'for any'

N is the set of natural numbers [0,1,2,...[

R is the set of real numbers]-∞, +∞[

Z is the set of integers]...,-3,-2,-1,0,1,2,...[

I.1 Introduction

In vertical seismic profiling (VSP) and other borehole seismic measurements, a cylindrical tool containing seismic sensors (geophones) is lowered into the borehole and clamped to the borehole's side. The coupling effect of this downhole tool on the observed seismic signals is of interest. In this paper we define the coupling as a filtering effect and determine the properties of this filter. We consider a filter with transfer function T, which has as input the seismic displacement and as output the measured displacement (Fig. 1). The determination of T depends upon the calculation of the dynamic radiation compliance I of the tool.

The geophone-ground coupling on a semi-infinite half space, for normal incidence of compressional waves, has been treated by several authors. Among them, Lamer (1970) represents the coupling by a damped oscillatory system which is shown to be equivalent to a second order low-pass filter. The resonance frequency of this filter depends essentially on the density and on the shear wave velocity of the ground, on the mass and on the contact surface of the geophone. Safar (1978) shows that the mutual interaction of a geophone set, resulting from the re-radiation of incident compressional waves, can have a considerable effect on the response of each geophone.

The calculation of circular footings and infinite-strip compliances on a semi-infinite solid has been undertaken by many authors, among whom Bycroft (1954), Gladwell (1968), Luco and Westmann (1971), and Miller and Pursey (1954).

In this first part we attempt to model the observed low frequency (15-30 Hz) oscillation encountered by a Schlumberger seismic measurement in a borehole, when the tool (WST) was clamped in a very soft formation. Analysis of VSP data is the initial step in the study of this effect. We shall consider a priori that the atypical signals might result from relatively "poor" tool-borehole wall coupling. We will try to understand the effect of different parameters. However, since both of our theoretical models are simplified and far from the real geometry, our results are qualitative. Other possible interpretations are suggested for a future deeper investigation.

I.2 Observation & Data analysis

The VSP measurement consists of three main parts:

(i) The surface source.

The surface source is a Bolt DHS 1900 airgun, connected to a compressor. A pressure hydrophone in the vicinity of the source records the time and shape of the source signal.

(ii) The downhole tool. (Fig. 2)

The downhole seismic tool (WST) is cylindrical in shape. The tool's weight is about 125 kg, its length and diameter are 5m and 15 cm, respectively. The tool is positioned against the borehole wall by two arms activated by a hydraulic pump located at the top of the tool. This device is controlled from the surface. The tool is anchored by its own weight. Two 10cm-long rings, about 120 cm apart, are attached to the tool to prevent excessive adherence to soft formations.

The signal is recorded by 4 vertical Geospace HS1 velocity geophones (bandwidth 10-200 Hz at 3 dB). The downhole amplifier has a gain of 60 dB with a bandwidth of 0-2 kHz at 3 dB.

(iii) Recording System.

The recording is made by a Cyber Service Unit (CSU) on the surface. The vertical distance between two tool positions corresponds to 8 ms (125 Hz) in vertical travel time (approximately 20 m for compressional wave velocity V_p = 2500 m/s). Other characteristics of the surface recording are:

Low cut and anti-aliasing	0.5 - 250 Hz at 3 dB	
Downhole signal sampled at	1 ms	(1 kHz)
Surface sensor sampled at	0.5 ms	(2 kHz)

About 3 seconds of signal is recorded for each shot.

Recordings with no offset shooting have been made in Test well X (Fig. 3). Different depths, with known lithologies were investigated. Representative data have been selected for presentation in this section:

Fig. 4 contains 5 typical signals, and some of their amplitude spectrums obtained in this well. Fig. 5 shows signals recorded in uncased limestone (A) and shales (B and C). Fig. 5 (B)&(C) shales are about 44 m deeper than the limestone in (A). In Fig. 5 (B), the dominant phase is the tube waves. Since the gain is adjusted on the basis of maximum amplitude, the body wave arrivals that have small amplitudes cannot be seen. To look at the body waves in detail we plotted the interval 400-900 ms with much higher gain in Fig. 5 (C). The P-wave signal is weak and the waveform is oscillatory. In the Fourier amplitude spectra (Fig. 7 and 8 (B)) we can see the effects of oscillations and an attenuation of frequencies above 50 Hz, compared to those in Fig. 5(A) and 7&8 (A). Similar characteristics are seen in Fig. 4 (D) & (E).
Signals of Fig. 5 (A) and (C) when filtered with a 10-80 Hz band-pass filter give Fig. 6 (A) and (B). The difference between limestone and shale signals is further emphasized in this figure 6.

Properties of these atypical shale signals (Fig. 4 (D) and (E), Fig. 5 (B) and (C)) and of their amplitude spectrums can be summarized into 3 main characteristics:

- attenuation of high frequencies ($\gtrsim$ 50 Hz)
- large amplification of tube waves
- loss of signal in noise.

Since these odd signals exist only in a "soft" formation, it is natural, a priori, to attribute this effect to the tool-formation coupling. We shall therefore follow this path to see if the models can explain the observed data.

I.3 Resonance Models

The aim of the models is to evaluate the transfer function T of the coupling linear filter, for reasonable values of the physical properties of both the formation and the tool. The first model Axicylin (section I.4) computes T from a vibrating rigid cylinder. The second model Infistrip (section I.5) which is simpler (limiting case of Axicylin when the radius $\to \infty$), computes T from a vibrating rigid infinite strip.

Our assumptions are the following:
(1) The WST downhole tool is welded to the formation during dynamic excitation (strong and debatable assumption, see Appendix A for more details)(displacements, involved 10^{-8}-10^{-7} m), (2) the medium near the tool is homogeneous, isotropic and linear elastic, (3) the tool is rigid, (4) time dependence is of the form exp $(-i\omega t)$, (5) there is no offset shooting, and (6) the tool is excited by a vertical shear stress only.

Since we only have vertical geophones, we will limit our interest to the vertical component w of the displacement vector $\underset{\sim}{u} = (u,v,w)$.

Parameter definitions:

The formation and the tool parameters that need to be used in modelling are listed below along with typical values.

(i) Formation parameters:

Poisson's ratio	ν	($\lesssim .40$)
Compressional wave velocity	V_p	(~3000 m/s)

Mean density	ρ	(~2000 kg/m^3)
Borehole radius	a	(~.15 m)
Spring elastic constant	K	?
Dashpot damping constant	η	?

(ii) Tool parameters:

Total mass	M	(~125 kg)
Distance between the two rings	L	(~ 120 cm)
Length of contact tool-borehole wall	DD	(~ 20 cm)
Width of contact (circular for Axicylin) (linear for Infistrip)	δ	($\lesssim$ 6 cm)

We shall limit our study to the frequency range 10-200 Hz. In this range, the amplitude spectrum of the geophones is nearly constant at unity.

Defining w^s as the seismic displacement along z on the contact surface, in the absence of the tool, and w^t the displacement along z on the contact surface due to the tool's excitation (tool's vibration considered as a source), the seismometer output is then $w = w^s + w^t$ (total displacement).

The transfer function T of the coupling (along z) is defined as (Fig. 9)

$$T \equiv \frac{w^s + w^t}{w^s} = \frac{w}{w^s} \quad . \tag{3.1}$$

N.B. If we have a perfect coupling, $w^t=0$ and T=1.

Since we are considering only the vertical displacement,

T is the transfer function for the vertical component.

The shortest wavelength is (for V_p ~ 3000 m/s) $\lambda_{min} = \frac{3000 \text{ m/s}}{200 \text{ Hz}} = 15$ m, and $\lambda_{min} >> L$. We will therefore assume that on the surface of contact DD the shear stress σ_{rz} produced by the incoming wave does not vary (i.e. σ_{rz} is constant at fixed time on the tool's contact surface) .

The tool-formation coupling can be well understood by considering its equivalent oscillatory system (Appendix B), where

$$T(\omega) = \frac{1}{1 - M\omega^2 (K - i\omega\eta)^{-1}} \quad . \qquad (3.2)$$

Unfortunately, this method provides only a good physical support since we are unable to determine K and η. Hence the following step is to compute T via the radiation of the tool (Appendix C). If $I^t(\omega)$ is the radiation compliance of the tool for a given surface of contact $\delta \cdot DD$, we get

$$T(\omega) = \frac{1}{1 - M\omega^2 I^t(\omega)(\delta \cdot DD)^{-1}} \quad . \qquad (3.3)$$

These two equations (3.2 and 3.3) are equivalent. In the radiation case (3.3) we need to specify $\delta \cdot DD$ and $I^t(\omega)$. In the oscillation formula (3.2) we need to give K and η .

I.4 Model AXICYLIN

In model Axicylin the tool is represented by a rigid vibrating cylinder of finite length DD, excited along its vertical axis (Fig. 10) . The cylinder is welded on the inner surface of an infinite cylindrical hole of radius a, in a linear-elastic, homogeneous and isotropic medium. $I^c(\omega)$ of the cylinder will be computed. Approximate values of the tool's compliance $I^t(\omega)$ and the transfer function T of the coupling will be derived.

The problem is axisymmetric. We shall consider homogeneous boundary conditions in stress. Time dependence $e^{-i\omega t}$ will be omitted throughout the formulation.

Boundary conditions at r = a, are (see Fig. 11) in cylindrical coordinates (r,z):

$$\begin{aligned} \sigma_{rz} &= s \quad \text{(constant)} && z < |d| \\ &= 0 && z > |d| \end{aligned} \qquad (4.1)$$

$$\sigma_{rr} = 0 \qquad \forall\, z$$

Solving the wave equation in cylindrical coordinates (r,θ,z), via the seismic potentials, and considering the symmetry properties we get after some tedious manipulations, the z component of the displacement vector $\underset{\sim}{u}^t = (u^t,v^t,w^t)$ (see Appendix D).

We compute $w^t(r=a,z)$ and take the mean value along DD,

$$\langle w^t \rangle = 2 \int_0^\infty \{i\xi\, A_o(\xi)\, H_o(ha) + k^2\, Co(\xi)\, H_o(ka)\} \sin(\xi d)/(\xi d)\, d\xi \qquad (4.2)$$

with

$$A_o(\xi) = \frac{2is\,[k\, H_o(ka) - H_1(ka)/a\,]\sin(\xi d)}{\pi\mu\, R(\xi)},$$

and

$$C_o(\xi) = \frac{s\,[2h\, H_1(ha)/a - (k_\beta{}^2 - 2\xi^2)\, H_o(ha)]\sin(\xi d)}{\pi\xi\mu k\, R(\xi)},$$

where $R(\xi) \equiv H_1(ka)\, H_o(ha)\, (2\xi^2 - k_\beta{}^2)^2 + H_1(ha)\, Ho(ka)\, 4hk\xi^2$

$$- 2hk_\beta{}^2\, H_1(ha)\, H_1(ka)/a.$$

Hence $$I^c = \frac{\langle w^t \rangle}{\sigma_{rz}} = \frac{\langle w^t \rangle}{s}. \qquad (4.3)$$

$I^c(\omega)$ is the radiation compliance of the whole cylinder having $2\pi a.DD$ for contact surface, let M^c be its mass.

Use of (C.4) gives

$$T^c(\omega) = \frac{1}{1 - M^c\omega^2\, \dfrac{I^c(\omega)}{(2\pi a.DD)}}. \qquad (4.4)$$

What we would like to evaluate is

$$T(\omega) = \frac{1}{1 - M\omega^2 \frac{I^t(\omega)}{(\delta.DD)}} \quad , \tag{4.5}$$

where $I^t(\omega)$ is the compliance of the tool having $\delta \cdot DD$ as contact surface.

Fortunately, we can compare $I^c(\omega)$ and $I^t(\omega)$. $I^c(\omega)$ applies to a contact surface $S_1 = 2\pi a.DD$ wich is greater than the contact surface $S_2 = \delta.DD$ of $I^t(\omega)$, and

$I = \frac{\langle w \rangle}{\sigma_{rz}}$ where σ_{rz} is constant for I^c and I^t.

Applying the fundamental law of dynamics for M^c and M we get

$$F_1 = \sigma_{rz}.S_1 = M^c \langle \ddot{w}_1 \rangle \text{ and } F_2 = \sigma_{rz}.S_2 = M \langle \ddot{w}_2 \rangle .$$

In order to get $I^c \sim I^t$ we must have $\langle w_1 \rangle \sim \langle w_2 \rangle$, or

$$F_1 / F_2 = M^c / M. \tag{4.6}$$

Since σ_{rz} is constant, (4.6) reduces to

$$S_1 / S_2 = M^c / M. \tag{4.7}$$

Assuming that $M^c = \frac{2\pi a}{\delta} M$, (4.7) is satisfied.

Hence $$I^t(\omega) \sim I^c(\omega) \tag{4.8}$$

Therefore the transfer function tool-formation given by (4.5) is approximated by

$$T(\omega) \sim \frac{1}{1 - M\omega^2 \frac{I^c(\omega)}{\delta.DD}} \quad . \qquad (4.9)$$

The tool's resonance frequency is

$$f_R{}^t \sim \frac{1}{2\pi} \left(\frac{\delta.DD}{M\ I^c(\omega_R)} \right)^{1/2} \quad . \qquad (4.10)$$

It is interesting to note that (4.4) can be directly applicable to the problem of a casing not well cemented if $DD << \lambda_{min}$; since DD~10m then we must restrict our frequency range to [10,100]Hz and λ_{min}~30m. Thus we will have at least qualitative information from (4.4). The quality of cementing can be specified by then fractional surface S coupled to the formation. When we have good cementing S ~$2\pi a.DD$. For poor cementing S <$2\pi a.DD$.

Numerical details of the formulation are briefly exposed in Appendix F.

I.5 Model INFISTRIP

This model approximates the borehole surface with a plane surface and the tool as a portion of an infinitely long strip (infinite in y) welded to the plane. The axis of the borehole is parallel to the z direction of the plane (see Fig. 10).

The problem of an infinitely long strip of finite width DD vibrating tangentially to the free surface of a medium and normally to the axis of the strip has been studied by Miller and Pursey (1954).

The boundary conditions at the free surface x=0, are (see Fig. 12) in cartesian coordinates (x,z)

$$\begin{aligned} \sigma_{xz} &= s \quad \text{(constant)} && z < |d| \\ &= 0 && z > |d| \end{aligned} \qquad (5.1)$$

$$\sigma_{xx} = 0 \qquad \forall\, z \qquad (DD=2d)$$

Since we are only interested on the tangential component w^t of the displacement vector $\underset{\sim}{u}^t=(u^t,w^t)$ when the tool vibrates, we get for the mean value $\langle w^t \rangle$ along DD, at x=0 (see Appendix E)

$$\langle w^t \rangle = \frac{s\ DD}{\pi\mu} \int_0^\infty \frac{k_\beta^2 (\xi^2-k_\beta^2)^{1/2}}{F(\xi)} \frac{\sin^2(\xi d)}{(\xi d)^2}\, d\xi \qquad (5.2)$$

where $F(\xi) = (2\xi^2-k_\beta^2)2 - 4\xi^2\ (\xi^2-k_\alpha^2)^{1/2}\ (\xi^2-k_\beta^2)^{1/2}$

It is shown in Appendix G that Infistrip is a particular case of Axicylin when $a \to \infty$.

Hence $$I^s = \frac{\langle w^t \rangle}{\sigma_{rz}} = \frac{\langle w^t \rangle}{s} \quad . \qquad (5.3)$$

$I^s(\omega)$ is the radiation compliance of the strip. Set S and M^s the surface and the mass of the strip, respectively.

Use of (C.4) gives

$$T^s(\omega) = \frac{1}{1 - M^s \omega^2 \frac{I^s(\omega)}{S}} \quad . \qquad (5.4)$$

However, since the strip is infinite we have then to define a strip surface density ρ^s. Thus $M^s \equiv S\ \rho^s$. (5.5)
Use of (5.5) in (5.4) gives

$$T^s(\omega) = \frac{1}{1 - \rho^s\ \omega^2\ I^s(\omega)} \quad . \qquad (5.6)$$

Again as in (4.5), what we are looking for is

$$T(\omega) = \frac{1}{1 - M\omega^2 \frac{I^t(\omega)}{(\delta.DD)}} \quad , \qquad (4.5)$$

where $I^t(\omega)$ is the compliance of the tool having $\delta \cdot DD$ as contact surface.

By the same token as in section I.4, if we assume $\rho^s = M/(\delta.DD)$ as surface density of the strip, we get

$I^t(\omega) \sim I^s(\omega)$. We therefore can approximate $T(\omega)$ by $T^s(\omega)$ in (4.5),

$$T(\omega) \sim \frac{1}{1 - M\omega^2 \frac{I^s(\omega)}{(\delta.DD)}} \quad . \tag{5.7}$$

The tool's resonance frequency is

$$f_R{}^t \sim \frac{1}{2\pi} \left(\frac{\delta.DD}{M\ I^s(\omega_R)} \right)^{1/2} \quad . \tag{5.8}$$

For the numerical details of the formulation see Appendix F.

I.6 Results and Discussion

We calculated a suite of models to determine the transfer function T for different tools and formations, and the sensitivity of the results to different model parameters.

Consider reference models with initial values of parameters (ex: Fig. 13 for Axicylin and Fig. 17 for Infistrip). The sensitivity to each parameter, is determined by varying the particular parameter while keeping all others constant. These effects are studied in detail with the computation of numerous models. The results are condensed in Tables 1 and 2. The notation used in the tables are as follows:

Let us define LFR as "lower resonance frequency"

↗ as an increase (ex: M↗ means M increases)

↘ as a decrease.

\- as a an insignificant variation .

Table 1.

Model Axicylin

Parameter	Resonance Peak	Halfwidth f1/2	Max amplitude
M ↗	LFR	↘	↗
ν ↗	LFR	↘	-

Parameter	Resonance Peak	Halfwidth f1/2	Max amplitude
V_p ↘	LFR	↘	-
ρ ↘	LFR	↘	-
a ↗	LFR	↗	↘
δ ↘	LFR	↘	↗
DD ↘	LFR	↘	↗

Table 2.

Model Infistrip

Parameter	Resonance Peak	Halfwidth f1/2	Max amplitude
M ↗	LFR	↘	↗
ν ↗	LFR	↘	-
V_p ↘	LFR	↘	-
ρ ↘	LFR	↘	-
δ ↘	LFR	↘	↗
DD ↘	LFR	↘	↗

From the tables we can immediately deduce some conclusions. The parameters that could be controlled in designing a new tool are: M, δ, DD and L.

In order to have a good coupling and move the resonnance peak away from the seismic frequency band of interest we should decrease the mass of the tool M, increase its surface of contact δ.DD and decrease the distance L between the two rings. (increasing L will invalidate the approximation $\lambda_{min} \sim 10$ L, wich is a necessary condition in our formulation. Furthermore, interferences between the two rings may occur for $L > \lambda_{min} / 2$)

We calcuated the transfer functions for two types of formations: A soft formation (shale) with $\nu = .4$, $V_p = 3000$ m/s, $\rho = 2000$ kg/m^3 and a hard formation (limestone) with $\nu = .25$, $V_p = 4500$ m/s, $\rho = 2500$ kg/m^3. The tool is the WST with M = 125 kg, DD = 20 cm and 1 cm $< \delta <$ 6 cm.

Amplitude spectrums of these two formations are plotted:

Axicylin model:

Fig. 13 corresponds to a soft formation with δ = 2 cm, Fig. 14 with δ = 4 cm and Fig. 15 with δ = 6 cm.

Fig. 16 corresponds to a hard formation with δ = 1 cm.

Infistrip model:

Fig. 17 represents the case of a soft formation with δ = 2 cm, Fig. 18 with δ = 4 cm and Fig. 19 with δ = 6 cm.

Fig. 20 corresponds to a hard formation with δ = 2 cm.

The main difference between the two models Axicylin and Infistrip is that the latter does not take into account the curvature of the borehole. This results for Infistrip (compared to Axicylin) in:

- a shift of the resonance frequency towards low frequencies
- a larger half-width of the curve
- a lower maximum peak resonance

These differences are not surprising since Infistrip is a limiting case of Axicylin when the radius of the borehole tends to infinity. Therefore using the sensitivity analysis of Axicylin for the radius a, by increasing it we deduce these same differences between Infistrip and Axicylin. The model Axicylin is therefore more appropriate to consider since it includes information about the borehole's curvature.

The resonance frequencies resulting from our model are above 100 Hz. Therefore we are not able to fit the observed data with our model for plausible physical values. From all our assumptions, the one which is the most debatable is the welding condition: the tool is welded to the wall of the borehole for any formation during dynamic excitation. Dynamic slipping might be present in soft formation when the tool is anchored by its own weight (A.2 not satisfied). If slipping occurs (probably on the opposite side of the arms), the seismometer will be sensitive to the motion in the fluid. Hence, it will record signals resulting from motions in the formation and in the

fluid. Since the vertical component of the tube wave in the fluid is on the order of 10 times the one in the formation (Fig. 21, Cheng and Toksöz 1981), these tube waves can induce motion in a poorly anchored borehole seismometer.

I have attempted to fit the observation on the basis of a resonance effect of a well anchored tool. A similar model which would include slipping of the tool and tube wave contribution might satisfy the observations, and thus explain the cause of these atypical signals.

Other additional effects can be the presence of noise in the soft formation due to a low frequency permanent noise and/or noise due to P and S waves converted into tube waves close to the tool (Cheng and Toksöz 1981).

I.7 Conclusions

The conditions, for a better coupled tool with the formation inferred from our models are:

Positive anchoring (A.2)

Rigid tool (assumption (3))

Minimize the tool's mass M ↘

Increase the contact surface tool-formation δ.DD ↗

Decrease the distance between the two rings L ↘

The two models were not able to explain the observed odd signals for reasonable physical values. It seems probable that the tool is sometimes not well anchored to the borehole wall for soft formations. This results in an observed large amplitude tube wave displacement, indicative of poor anchoring. Other additional effects can be due to the presence of low frequency pre-existing noise and/or generated tube waves by body waves incident on the borehole in the vicinity of the tool. A new model which would take into account the slipping of the tool and the tube wave effect will be the next step in studying the tool-formation coupling.

Part II

TUBE WAVE GENERATION FROM A FLUID-FILLED FRACTURE

List of Symbols

c = Tube wave phase velocity

f = frequency

$I_i(z)$, $K_i(z)$ = modified Bessel functions of the ith order

K = permeability

k = ω/c vertical wavenumber

$L(t)$ = Fracture width

L_o = Maximum fracture width

$\ell = k(1-c^2/\alpha^2)^{1/2}$ radial wavenumber from P wave contribution

$m = k(1 - c^2/\beta^2)^{1/2}$ radial wavenumber from S wave contribution

$n = k(1 - c^2/\alpha_f^2)^{1/2}$ radial wavenumber from fluid P wave contribution

R = borehole radius

u_z^{α} = vertical displacement of the compressional (P) wave in the formation

u_z^T = Tube wave vertical displacement in the formation

u_{fz}^T = Tube wave vertical displacement in the borehole fluid

V_s = shear (S) wave velocity in the formation

α = compressional (P) wave velocity in the formation

α_f = compressional (P) wave velocity in the borehole fluid

$\beta = -\frac{1}{v}\left(\frac{\partial v}{\partial P}\right)_T$ fluid compressibility

$\varepsilon(t)$ = fracture wall displacement

ε_{ii} = volumetric strain of tube waves in the borehole fluid

ε_o = Maximum fracture wall displacement

η = dynamic viscosity

ρ = formation density

ρ_f = fluid density

$\omega = 2\pi f$ angular frequency

II.1 Introduction

In part I we discussed seismic noise due to the oscillation of the tool. In this section we will present a source of noise which is independent of the tool. A compressional body wave impinging on a fractured zone penetrated by an uncased borehole would generate tube waves. This concept of localizing permeable zones from the tube wave analysis in VSP data has been proposed by Huang and Hunter (1981). The closure of a fluid filled fracture due to an incident compressional wave would inject an amount of fluid in the borehole. This fluid movement is the source of excitation of tube waves. At this location, two tube waves will propagate, one up the borehole and one downwards. Such an observation in a VSP section would lead to the determination of a high permeable zone intersecting the borehole.

For a first consideration of this fluid mechanism mathematically, some idealized geometry must be adopted. The geometry we have chosen is that of a parallel-walled fracture which intersects the borehole normal to the borehole axis, with a compressional sinusoidal plane wave impinging normally on the fracture. We will first calculate the volume of fluid ejected from the fracture during the first one-fourth period of the incident wave. Then, we evaluate the tube wave displacement generated by the squirting of the fluid. The in-situ fracture width can be estimated from the ratio of the tube wave amplitude to the P wave amplitude.

II.2 Fracture model

Consider the specific example of a parallel-walled fluid-filled fracture (with low aspect (thickness to length) ratio $<<10^{-3}$). The fracture is penetrated normally by an uncased borehole. The fluid in the fracture is in hydrostatic equilibrium with the fluid in the borehole when there exists no perturbation.

An incident P wave impinges normally on the fracture, exciting it sinusoidally. The wavelength of the disturbance is assumed to be much greater than the thickness of the cavity .

For very small strains, the fracture width L(t) is assumed to oscillate about the static shape L_o as

$$L(t) = L_o - \varepsilon(t) \qquad (2.1)$$

where $\varepsilon(t) = \varepsilon_o \sin\omega t$ and $\varepsilon_o << L_o$,

ε_o is the maximum fracture displacement (Fig. 22).

Other assumptions are: we are in the low frequency approximation therefore in the presence of laminar flow and use of Darcy's law is then valid. The flow is essentially one dimensional. The medium is rigid compared to the fluid. The fluid squirted into the borehole does not perturb significantly the borehole pressure $P_o = \rho_f gh$ (h is the height of fluid in the borehole at the point of measure, g is the gravitational acceleration).

From classical fluid mechanics (ex: Landau and

Lifshitz, 1959) we can derive the permeability of two parallel planes separated by L and enclosing the fluid. We obtain

$$K = \frac{L^2}{12}$$

Since we assumed the wavelength of the oscillation to be much greater than the width of the cavity and $\varepsilon_o << L_o$, the quasi-static approximation may be employed to represent the time dependent permeability

$$K(t) = \frac{L^2(t)}{12}$$

For convenience we shall take the time average of K(t) in the first one-fourth period of the incident wave (T/4), i.e.

$$\overline{K} = \frac{4}{T} \int_o^{T/4} L^2(t)dt$$

$$\overline{K} = \frac{L_o^2}{12} - \frac{2\varepsilon_o L_o}{\pi} \qquad (2.2)$$

The rate at which fluid flows in the presence of a pressure gradient $\partial p/\partial x$ is related by Darcy's Law to the cross sectional area L(t), the fluid viscosity η and the permeability $\overline{K}$

$$q = - \frac{\overline{K}L(t)}{\eta} \frac{\partial p}{\partial x} \qquad (2.3)$$

During a time increment dt, a differential volume element $dx \cdot L(t)$ stores a certain amount of fluid.

The elementary volume entering at $x = \xi - dx$ is (Fig. 23)

$$q_1 \, dt = - \frac{\overline{K}}{\eta} L(t) \frac{\partial p}{\partial x} \, dt \qquad (2.4)$$

The elementary volume exiting at $x = \xi$ is

$$q_2 dt = - \{\frac{\overline{K}}{\eta} L(t) \frac{\partial p}{\partial x} + \frac{\partial}{\partial x}(\frac{\overline{K}}{\eta} L(t) \frac{\partial p}{\partial x}) dx\} \, dt \qquad (2.5)$$

The net storage of fluid in $dx.L(t)$ is due to the fluid ejected from the fracture's closure and the compressibility of the fluid. During a time increment dt this total storage is

$$\frac{-d\varepsilon(t)}{dt} \, dxdt + L(t) \beta \, (\frac{\partial p}{\partial t}) dxdt \qquad (2.6)$$

The net storage given by (2.6) must equal the net volume $(q_1 - q_2)dt$. Use of (2.4) and (2.5) with (2.6) gives

$$\frac{\partial}{\partial x} \, (\frac{\overline{K}}{\eta} L(t) \frac{\partial p}{\partial x}) = L(t) \beta \, \frac{\partial p}{\partial t} - \dot{\varepsilon}(t)$$

where $\dot{\varepsilon}(t) = \frac{d\varepsilon(t)}{dt} = \omega \varepsilon_o \cos \omega t$.

Setting $a^2 = \frac{\overline{K}}{\eta \beta}$ and $q(t) = \frac{-\dot{\varepsilon}(t)}{\beta L(t)}$ we get

$$a^2 \frac{\partial^2 p}{\partial x^2} - \frac{\partial p}{\partial t} = q(t), \qquad (2.7)$$

with the boundary condition in pressure

$$p(x,t=o) = P_o \quad \forall x>o$$

$$p(x=o,t) = P_o \quad \forall t>o$$

$$\frac{\partial p}{\partial x}\Big|_{x=\infty} = 0.$$

The last condition states that there is no fluid flow in the fracture far from the borehole intersection.

Equation (2.7) is a one-dimensional inhomogeneous diffusion equation. The heat conduction analogy corresponds to a semi-infinite half-space (x>o) having a^2 as thermal diffusivity and a time varying heat source q(t). The solution to this partial differential equation (2.7) is (Appendix H),

$$p(x,t) = P_o - \int_o^t q(t-\tau)\,\mathrm{erf}\left(\frac{x}{2a\sqrt{\tau}}\right)d\tau \qquad (2.8)$$

where $\mathrm{erf}(z) = \frac{2}{\sqrt{\pi}} \int_o^z e^{-t^2}dt$ is the Error function.

Note that for large x, $p(\infty,t) = P_o + \frac{1}{\beta} \ell n \frac{L(t)}{L_o}$.

The pressure gradient $\partial p/\partial x$ is then from (2.8)

$$\frac{\partial p}{\partial x}(x,t) = -\frac{1}{a\sqrt{\pi}} \int_o^t q(t-\tau)\exp(-x^2/4a^2\tau)\ \tau^{-1/2}d\tau \qquad (2.9)$$

The rate at which fluid flows is from (2.3)

$$q(x,t) = -\frac{\bar{K}L(t)}{\bar{\eta}} \frac{\partial p(x,t)}{\partial x} \quad .$$

We wish to calculate the volume ejected from the fracture for the maximum fracture displacement. This would lead to a maximum volume ejected in a finite amount of time which characterizes the dynamics and the tube wave displacement. Thus, we have to minimize (2.1). This maximum volume occurs for $t = T/4 = 8\pi/\omega$ which gives $L(T/4) = L_o - \varepsilon_o$. Therefore the volume of fluid forced into the borehole from the fracture is

$$\Delta V = \int_o^{T/4} q(x=o,t)dt \qquad (2.10)$$

or explicitly,

$$\Delta V = \varepsilon_o L_o \left(\frac{1}{12\pi\beta\eta}\right)^{1/2} F(\omega, \varepsilon_o/L_o) \qquad (2.11)$$

where $F(\omega, \varepsilon_o/L_o) = \omega \int_o^{T/4} \int_o^t \frac{1 - \varepsilon_o/L_o \sin\omega t}{1 - \varepsilon_o/L_o \sin\omega\tau} \frac{\cos\omega\tau}{(t-\tau)^{1/2}} d\tau dt$

Computation shows that for increasing frequency, $F(\omega, \varepsilon_o/L_o)$ decreases. This is consistent with the fact that as the frequency increases more fluid is compressed and therefore the ejected fluid volume decreases.

For $\varepsilon_o <<< L_o$ we can use an asymptotic expression for $F(\omega, \varepsilon_o/L_o)$.

$$F(\omega,o) = 2\omega \int_o^{T/4} (T/4-t)^{1/2} \cos\omega t dt \ .$$

The volume obtained in (2.11) is in two dimensions. Since in the real case we are in a 3D configuration and the 3D complete solution is beyond the scope of this study, two approximate 3D extrapolations will be considered.

(1) A fracture with the geometry of a strip having about 2R as horizontal length (Figure 24.) intersects the borehole. Neglecting the edge effects during the flow, the 3D volume is approximately equal to

$$\Delta V_{3D} \cong 4R\ \Delta V, \qquad (2.12)$$

R being the radius of the borehole. ΔV_{3D} is a lower bound of a fracture which extends around the borehole.

(2) The 2D and 3D problems beeing solved for a stationary process, we can use the results for this study with the low frequency approximation. This gives (Appendix I) for the fracture with a circular geometry around the borehole

$$\Delta V_{3D} \cong 2\pi R\ \chi\ \Delta V \qquad (2.13)$$

χ is the geometrical factor depending on the effective length d of the fracture and on the borehole radius R.

$$\chi = \frac{d/R}{\ln\left(\frac{R+d}{R}\right)} \quad .$$

II.3 Tube wave amplitude

Tube waves in VSP are low frequency Stoneley waves. These are interface or guided waves with the largest amplitude confined to the neighborhood of the solid-fluid boundary and decaying exponentially away from it. The dominant phase in a seismic signal recorded by a hanging tool in a borehole are the tube waves. The fluid pulse ΔV_{3D} forced from the fracture into the borehole (during a time interval of T/4) would then generate mainly tube waves.

Considering the plane z=o as the plane of symmetry of the fracture (Fig. 22), the integration of the tube wave volumetric strain ε_{ii} in the borehole (at z=o) over the radial distance and in T/4 must equal the fluid volume ejected from the fracture ΔV_{3D}. In axisymmetric cylindrical coordinates we have

$$\Delta V_{3D} = 2\pi c \int_0^R \int_0^{T/4} \varepsilon_{ii}(r,t,z=o)\, r\,dr\,dt \qquad (3.1)$$

Using the seismic potentials for tube waves given by Cheng and Toksöz (1981) (Appendix J) we can calculate ε_{ii} and evaluate the tube wave displacement in the borehole fluid. We are interested in the amplitude of the vertical component of displacement $|u^T_{fz}|$,

we get $$|u^T_{fz}| = C\, k\, I_o(nr) \qquad r < R^- \qquad (3.2)$$

where $$C = \frac{(1-c^2/\alpha f^2)^{1/2}}{2\pi R(2-c^2/\alpha_f^2) I_1(nR)} \quad \Delta V_{3D} \qquad (3.3)$$

From the tube wave amplitude (displacement) in the fluid $|u_{fz}^T|$ we can derive the tube wave amplitude in the formation $|u_z^T|$ (Appendix J). We get

$$|u_z^T| = A[kK_o(\ell r)+mGK_o(mr)] \quad r > R^+ \tag{3.4}$$

where

$$G = \frac{2\ell V_s^2 K_1(\ell R)}{k(c^2-2V_s^2)K_1(mR)} \tag{3.5}$$

and

$$A = \frac{n(2Vs^2-c^2)}{\ell c^2 K_1(\ell R)} \; I_1(nR) \; C \tag{3.6}$$

Consider now the inverse problem. Given the tube wave amplitude normalized to the direct P wave amplitude in the formation, the frequency of excitation, and the borehole and formation parameters, we can estimate the in-situ fracture width. The magnitude of the P wave displacement $|u_z^\alpha|$ is, in a first approximation, representative of ε_o (the maximum fracture displacement). In fact $|u_z^\alpha| < \varepsilon_o$ since the medium is not rigid and therefore the displacement close to the fracture is greater than the displacement far away from it. The ratio $\varepsilon_o/|u_z^\alpha|$ is representative of the fracture length and the stiffness of the formation. However in our formulation we shall assume $|u_z^\alpha| \sim \varepsilon_o$ which is equivalent in considering a lower bound of the fracture width L_o.

II.4 Results

We shall choose the frequency f to be 25 Hz, and the following values for the parameters:

Fluid incompressibility $\beta^{-1} = 2 \times 10^9$ Pa

Dynamic viscosity $\eta = 10^{-3}$ Poiseuille

Maximum fracture displacement $\varepsilon_o \sim |u_z{}^{\alpha}|$ $\quad \varepsilon_o << L_o$

Radius of borehole R = 0.1m

P-wave velocity of fluid $\alpha_f = 1500$ m/s

Fluid density $\rho_f = 1.2$ g/cm^3

Since we assumed the medium to be rigid compared to the fluid, ΔV_{3D} for the strip fracture (2.12) can be calculated for any formation:

$$F(\omega, \varepsilon_o/L_o) \simeq 0.156$$

and

$$\Delta V_{3D} \simeq 14.2 \times 10^3 \ \varepsilon_o L_o$$

We shall consider two types of formation:

(i) "Hard" with $\alpha = 4500$ m/s, $v_s = 2400$ m/s and $\rho = 2.3$ g/cm^3

(ii) "Sediment" with $\alpha = 2700$ m/s, $v_s = 1200$ m/s and $\rho = 2.1$ g/cm^3 .

The tube wave phase velocity c is calculated solving the period equation (Appendix J) for the given frequency and the formation and borehole parameters.

Results for the two formations are listed in Table 3. The ratio $|u_{fz}^T|/|u_z^T|$ is evaluated at r=R. If we are given $|u_z^T|/|u_z^{\alpha}| \sim |u_z^T|/\varepsilon_o$, the last column of Table 3 gives the value of the maximum fracture width L_o.

Table 4 gives some numerical values for L_o and the corresponding ratios $|u_z^T|/\varepsilon_o$ evaluated at $r = R^+$.

For a same amount of volume ejected from the fracture a "hard" formation would give a higher value of tube wave amplitude normalized to the direct P-wave amplitude. Two effects contribute to this increase:(1) the tube wave displacement in the fluid is greater in a "hard" formation than in a "sediment" (column 2 in Table 3) and (2) the ratio of tube wave amplitude in the fluid to that in the formation at r=R is larger in a "hard" formation (column 3 in Table 3).

The normalized tube wave amplitude decreases with decreasing frequency as shown for a "sediment" in Table 5. The volume forced into the borehole and the tube wave amplitude in the borehole fluid both increase with decreasing frequency. But the ratio of the tube wave amplitude in the fluid to that in the formation is so large for very low frequencies (10 Hz) that $|u_z^T|/\varepsilon_o$ varies in the same sense as the frequency.

See Appendix I for the results of the circular fracture in 3D (2.13). The normalized tube wave amplitudes are directly obtained by multiplying the values given by the strip fracture by $\pi\chi/2$.

Mavko and Nur (1979) give a limiting value for L_o, beyond which turbulent flow occurs. This maximum width is on the order of the millimeter for exploration frequencies. The fracture model is then qualitative for larger width.

Table 3.

(25 Hz)

Formation	$\lvert u^T_{fz} \rvert / \varepsilon_o L_o$	$\lvert u^T_{fz} \rvert / \lvert u_z^T \rvert$	$\lvert u_z^T \rvert / \varepsilon_o L_o$ at $r=R^+$ (m^{-1})
"Hard"	39×10^4	2380	165
"Sediment"	31×10^4	2218	140

Table 4.

(25 Hz)

L_o (mm)	"Hard" $\lvert u_z^T \rvert / \varepsilon_o$	"Sediment" $\lvert u_z^T \rvert / \varepsilon_o$
0.1	0.02	0.01
0.5	0.08	0.07
1	0.17	0.14
5	0.83	0.7
10	1.7	1.4

Table 5.

("Sediment")

f (Hz)	$\Delta V_{3D} / \varepsilon_o L_o$ (m)	$\lvert u^T_{fz} \rvert / \varepsilon_o L_o$	$\lvert u^T_{fz} \rvert / \lvert u_z^T \rvert$	$\lvert u_z^T \rvert / \varepsilon_o L_o$ at $r=R^+$ (m^{-1})
200	5.1×10^3	11×10^4	60	1816
100	7.2×10^3	15×10^4	195	790
50	10.1×10^3	22×10^4	644	337
25	14.4×10^3	31×10^4	2218	140
10	22.7×10^3	49×10^4	11 110	44

II.5 Conclusions

The fracture model estimated the in-situ width of a fluid-filled fracture given the ratio tube wave amplitude to P wave amplitude. The results seem to be consistent with the very scarce data in existence (Figure 25. Huang and Hunter, 1981). The values obtained are sensitive to frequency. For very low frequencies (less than about 15 Hz) and for a fracture width on the order of 1 mm the tube wave amplitude normalized to the P-wave amplitude is negligible in the formation.

The constraint that the formation is rigid compared to the fluid can be relaxed. The maximum fracture displacement ε_o would then depend on the formation parameters, the P wave displacement and on the extent of the fracture away from the borehole. A complete three dimensional approach, including axisymmetry seems possible.

Appendix A

ANCHORING CONDITION

Consider two bodies having a plane surface of contact. If we press them together by a force $\underset{\sim}{F}$ (amplitude F) normal to the plane of contact, then the shear force $\underset{\sim}{P}$ (amplitude P) parallel to the surface of contact, necessary to initiate sliding on it is given by Amonton's Law: (see fig. below)

$$P = c\,F$$

c being the static coefficient of friction.

The condition of no gravitational slipping is therefore

$$F\,c > P = Mg\ . \qquad \text{(A.1)}$$

M being the mass of the tool.

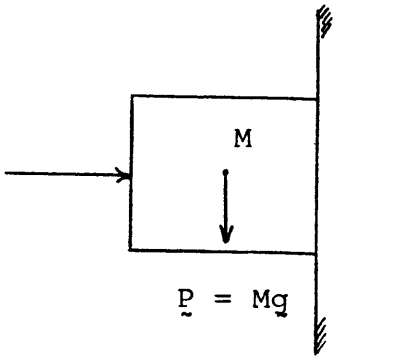

For soft formations, c ~ .25

To achieve (A.1) we must therefore have

$$F \sim 5P = 5\ Mg \sim 50\ M \quad \text{(Newtons)} \qquad \text{(A.2)}$$

This is not necessarily satisfied by the WST since it is anchored by its own weight. We however have no gravitational

slipping because on the extremity of the arms c is increased (presence of cleats). F here results from the weight of the tool (no positive anchoring force). If we have a positive anchoring force (i.e. (A.2) satisfied), we can foresee a better "welding" tool, in dynamic excitation, to formation than with no positive anchoring force (greater elimination of the mud-cake).

Appendix B

COUPLING OSCILLATORY SYSTEM

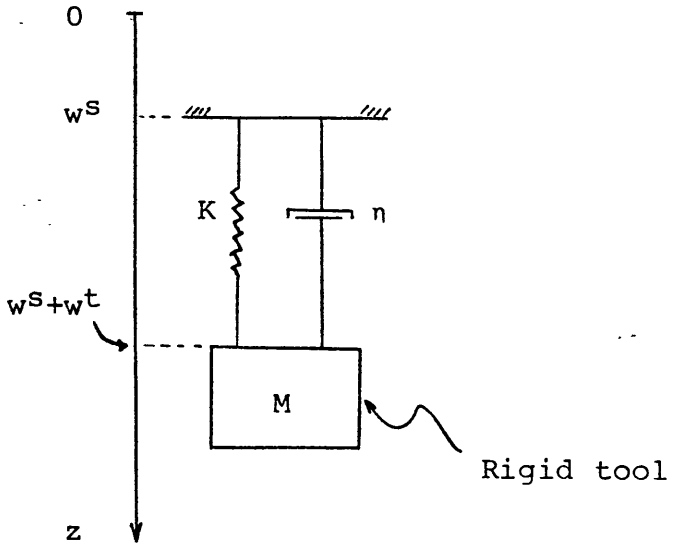

$w = w^s + w^t$

K is the spring elastic constant of the formation

η is the damping constant of the formation

All motion is restricted to the z-direction. The equation of motion of the following system is (see fig. above)

$$M\ddot{w} + \eta \dot{w}^t + K w^t = 0 . \qquad (B.1)$$

With $e^{-i\omega t}$ time dependence for w^s and w^t we obtain from (B.1),

$$-\omega^2 w - i\omega \eta/M (w - w^s) + K/M (w-w^s) = 0 . \qquad (B.2)$$

For $T = w / w^s$ we have from (B.2) the oscillatory T

$$T(\omega) = \frac{1}{1 - M\omega^2 (K-i\omega\eta)^{-1}} . \qquad (B.3)$$

N.B. For perfect coupling $K \to \infty$ (rigid medium) and $|T| = 1$.

Appendix C

RADIATION SYSTEM

Set F magnitude of force (generated by the incoming seismic wave and M) acting upon the formation from the tool ($F = \sigma_{rz} \cdot \delta \cdot DD$) F acts at the base of the tool.

$w \equiv w^t + w^s$ total displacement measured

$I^t(\omega) \equiv \frac{w^t}{\sigma_{rz}}$ dynamic radiation compliance of the contact surface of the tool.

N.B. $\sigma_{rz} = \frac{F}{\delta \cdot DD}$

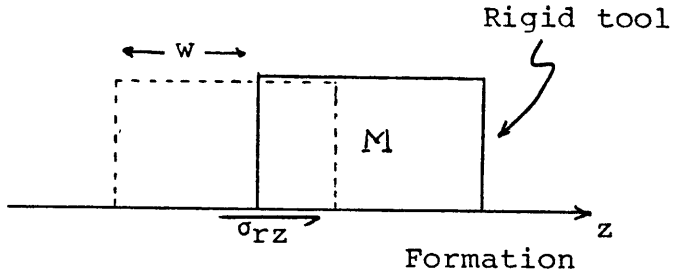

Applying the fundamental law of dynamics on the rigid tool with $e^{-i\omega t}$ time dependence, we get (see fig. above)

$$-F = -M\omega^2 w \qquad (C.1)$$

We have

$$w = w^s + \frac{FI(\omega)}{\delta \cdot DD} \qquad (C.2)$$

$$(C.2) \rightarrow \quad T(\omega) \equiv \frac{w}{w^s} = 1 + \frac{F \cdot I(\omega)}{\delta \cdot DD \cdot w^s} \qquad (C.3)$$

and (C.2) in (C.1) gives F which in (A3.3) gives the radiation T

$$T(\omega) = \frac{1}{1 - M\omega^2 I(\omega)(\delta \cdot DD)^{-1}} \quad . \qquad (C.4)$$

Appendix D

Formulation of AXICYLIN

In the elastic homogeneous medium, external to the borehole, the displacement field $\underset{\sim}{u}$ can be given in terms of scalar potentials Φ, Ψ and χ representing P-, SV- and SH- waves, respectively .

We have $$\underset{\sim}{u} = \nabla\Phi + \nabla x \nabla x(0,0,\Psi) + \nabla x(0,0,\chi) \quad . \qquad (D.1)$$

The first term gives the part which is free from rotation, and the second and third part are free from divergence.

The potentials satisfie the wave equation. Time dependance being $e^{-i\omega t}$, and in the absence of body force in the medium, these equations reduce to

$$\begin{aligned} \nabla^2\Phi &= -k_\alpha{}^2\Phi \\ \nabla^2\Psi &= -k_\beta{}^2\Psi \\ \nabla^2\chi &= -k_\beta{}^2\chi \quad . \end{aligned} \qquad (D.2)$$

In cylindrical coordinates (r, θ, z) we have $\underset{\sim}{u}=(u,v,w)$ and

$$\nabla^2 = \partial^2/\partial z^2 + 1/r.\partial/\partial r(r\partial/\partial r) + 1/r^2.\partial^2/\partial\theta^2 \qquad (D.3)$$

From (D.1) we have

$$\underset{\sim}{u} = \underset{\sim}{u}^P + \underset{\sim}{u}^{SV} + \underset{\sim}{u}^{SH} \qquad (D.3)$$

where

$$\underset{\sim}{u}^P = \left(\partial\Phi/\partial r \ , \ 1/r.\partial\Phi/\partial\theta \ , \ \partial\Phi/\partial z\right)$$

$$\underset{\sim}{u}^{SV} = \left(\partial^2\Psi/\partial r\partial z, \ 1/r.\partial^2\Psi/\partial z\partial\theta, -1/r.\partial/\partial r(r\partial\Psi/\partial r) - 1/r^2.\partial^2\Psi/\partial\theta^2\right)$$

$$\underset{\sim}{u}^{SH} = \left(1/r.\partial\chi/\partial\theta \ , -\partial\chi/\partial r \ , 0\right) \quad . \qquad (A4.4)$$

Expressing $\underset{\sim}{u}$ in terms of its components, we have

$$\underset{\sim}{u} = u\, r + v\, \theta + w\, z \qquad (D.5)$$

where

$$u = \partial\Phi/\partial r + \partial^2\Psi/\partial r\partial z + 1/r\ \partial\chi/\partial\theta$$

$$v = 1/r\ \partial\Phi/\partial\theta + 1/r\ \partial^2\Psi/\partial z\partial\theta - \partial\chi/\partial r$$

$$w = \partial\Phi/\partial z + \partial^2\Psi/\partial z^2 + k_\beta{}^2\Psi \quad \text{(using wave equ. for z-comp. of } \underset{\sim}{u}^{SV})$$

Looking for general solutions of the wave equations (D.2) that satisfy radiation conditions in the medium (i.e. wave must attenuate no slower than inverse distance far away from source, and wave must propagate outward to infinity), it follows that by the method of separation of variables they can be obtained by a superposition of the basic solutions (satisfying Bessel's equation) :

$$\phi_m(r,\theta,z,\xi) = A_m(\xi)\ e^{i\xi z}\ H_m(hr)\ e^{im\theta}$$

$$\psi_m(r,\theta,z,\xi) = C_m(\xi)\ e^{i\xi z}\ H_m(kr)\ e^{im\theta}$$

$$\chi_m(r,\theta,z,\xi) = B_m(\xi)\ e^{i\xi z}\ H_m(kr)\ e^{im\theta} \qquad (D.6)$$

$m \in Z$, and $\mathrm{Im}(h) \geq o$, $\mathrm{Im}(k) \geq o$.

We have the same vertical wave number ξ for P and S waves from the phase matching conditions at the interface r=a.

The gerneral solutions are obtained by super-imposing the basic solutions (D.6) :

$$\Phi(r,\theta,z) = \sum_{m\in Z} \int_R \phi_m(r,\theta,z,\xi)d\xi \quad \text{for P waves}$$

$$\Psi(r,\theta,z) = \sum_{m\in Z} \int_R \psi_m(r,\theta,z,\xi)d\xi \quad \text{for SV waves}$$

$$\chi(r,\theta,z) = \sum_{m\in Z} \int_R \chi_m(r,\theta,z,\xi)d\xi \quad \text{for SH waves.} \qquad (D.7)$$

The stress-displacement relations that we shall use are the following:

$$\sigma_{rr} = \lambda \operatorname{div} \underset{\sim}{u} + 2\mu \frac{\partial u}{\partial r}$$

$$\tau_{rz} = \mu \left[\frac{\partial w}{\partial r} + \frac{\partial u}{\partial z}\right] \quad . \qquad (D.8)$$

Let us show that the seismic potentials in this problem reduce to :

$$\phi(r,z,\xi) = A_o(\xi)\, e^{i\xi z}\, H_o(hr)$$

$$\psi(r,z,\xi) = C_o(\xi)\, e^{i\xi z}\, H_o(kr)$$

$$\chi(r,z,\xi) = 0 \quad . \qquad (D.9)$$

(i.e. only one modal contribution m=0 in (D.6) and no SH waves)

We can generalize the axial symmetry problem to a case with symmetry with respect to a vertical plane. Then, rotating the plane about a vertical axis, the axisymmetric case can be derived.

1- Symmetry with respect to a vertical plane (x0z) and vertical excitation. The components of the displacement vector $\underset{\sim}{u}$ satisfy (see fig. below)

$$u(\theta) = u(-\theta)$$
$$v(\theta) = -v(-\theta)$$
$$w(\theta) = w(-\theta) \ . \qquad (D.10)$$

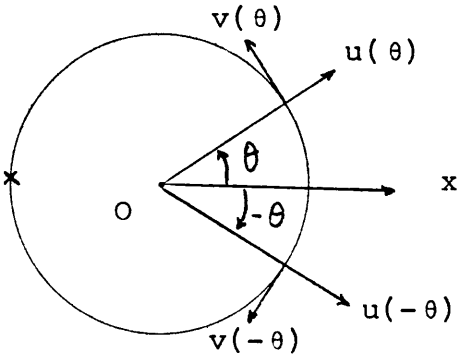

Recalling that $H_{-m}(\xi) = (-1)^m H_m(\xi)$, and expressing (u,v,w) in terms of the seismic potentials (D.7), and using (D.10) lead to a θ dependence of the following form

$$u(\theta) \sim \cos m\theta$$
$$v(\theta) \sim \sin m\theta$$
$$w(\theta) \sim \cos m\theta \qquad m \in Z \ . \qquad (D.11)$$

(D.11) is equivalent to a new definition of the seismic potentials:

$$\phi_m = A_m^*(\xi)\, e^{i\xi z}\, H_m(hr) \cos m\theta$$
$$\psi_m = C_m^*(\xi)\, e^{i\xi z}\, H_m(kr) \cos m\theta$$
$$\chi_m = B_m^*(\xi)\, e^{i\xi z}\, H_m(kr) \sin m\theta \qquad (D.12)$$

<u>where $m \in N$</u> (and not Z anymore) .

2- Axial symmetry with respect to the z axis. Vertical excitation. We get for $\underset{\sim}{u}$

$$u(\theta) = u(\theta + x\pi)$$
$$v(\theta) = 0 \qquad \forall\ x \in R$$
$$w(\theta) = w(\theta + x\pi) \quad ,$$

or equivalently,

u independant of θ
v = 0
w independant of θ . (D.13)

For a no θ dependance and v=0, the solution for the seismic potentials (D.12) is m=0, wich gives directly (D.9), with

$$A_o(\xi) \equiv A_o^*(\xi)$$
$$C_o(\xi) \equiv C_o^*(\xi)$$

The two unknowns of our problem to be determined are $A_o(\xi)$ and $C_o(\xi)$.

N.B. If our boundary conditions were plane symmetric, we can show that only m=1 would contribute in the seismic potentials (D.12). Ex: case of a disc vibrating tangentially on a semi-infinite solid.

With these potentials (D.9) we can now express explicitly σ_{rz} and σ_{rr} in function of $A_o(\xi)$ and $C_o(\xi)$, using (D.8), (D.5) (D.7) and (D.9):

$$\sigma_{rz} = \int_R F(\xi)\ e^{i\xi z}\ d\xi$$
$$\sigma_{rr} = \int_R G(\xi)\ e^{i\xi z}\ d\xi \qquad (D.14)$$

where

$$F(\xi) = \mu \{2hi\xi H_o'(ha) A_o(\xi) + (k_\beta^2 - 2\xi^2)k H_o'(ka) C_o(\xi)\}$$

$$G(\xi) = A_o(\xi) [2\mu h^2 H_o''(ha) - \lambda k_\alpha^2 Ho(ha)] + 2\mu i\xi k^2 H_o''(ka) C_o(\xi)$$

Use of the boundary conditions (4.1) with (D.14) leads to the following system :

$$\int_R F(\xi) e^{i\xi z} d\xi = s \qquad z < |d|$$

$$= 0 \qquad z > |d|$$

$$\int_R G(\xi) e^{i\xi z} d\xi = 0 \qquad \forall z \qquad \text{(D.15)}$$

From the properties of Fourier transforms, we will have an equivalent system

$$F(\xi) = \frac{s}{\pi} \cdot \frac{\sin\xi d}{\xi}$$

$$G(\xi) = 0 \qquad \text{(D.16)}$$

Solving (D.16) for $A_o(\xi)$ and $C_o(\xi)$, and rearranging the results for computational purposes, we get

$$A_o(\xi) = \frac{2is [k H_o(ka) - H_1(ka)/a] \sin(\xi d)}{\pi\mu R(\xi)}$$

$$C_o(\xi) = \frac{s\,[2h\,H_1(ha)/a - (k_\beta^2 - 2\xi^2)\,H_o(ha)\,]\,\sin(\xi d)}{\pi \xi \mu k\, R(\xi)} \qquad (D.17)$$

where $R(\xi) \equiv H_1(ka)\,H_o(ha)\,(2\xi^2 - k_\beta^2)^2 + H_1(ha)\,Ho(ka)\,4hk\xi^2 - 2hk_\beta^2\,H_1(ha)\,H_1(ka)/a.$

(n.b. when $a \to \infty$ we see Rayleigh function appearing multiplied by the factor $-2\,\frac{e^{ia(k+h)}}{\pi a\sqrt{hk}}$)

Therefore from (D.5) and (D.9) and (D.7) we get,

$$w(r,z) = \int_R \{i\xi\,A_o(\xi)\,H_o(hr) + k^2\,C_o(\xi)\,H_o(kr)\}\,e^{i\xi z}\,d\xi$$

Since $A_o(\xi) = -A_o(-\xi)$ and $C_o(\xi) = C_o(-\xi)$ we get,

$$w(r,z) = 2\int_0^\infty \{i\xi\,A_o(\xi)\,H_o(hr) + k^2\,Co(\xi)\,H_o(kr)\}\,\cos(\xi z)\,d\xi \qquad (D.18)$$

Taking the mean value of w along DD at r=a we get,

$$\langle w^t(r=a)\rangle \equiv \frac{1}{DD}\int_{-d}^{d} w^t(a,z)\,dz\,. \qquad (D.19)$$

Appendix E

Formulation of INFISTRIP

For the given boundary conditions (5.1), Miller and Pursey's paper gives the following final result for the Fourier transform of the z component of the displacement $\underset{\sim}{u}=(u,w)$ (cartesian coordinates, see Fig. 12)

$$w_F(x,\xi) = \frac{2s\ (\xi^2-k_\beta^2)^{1/2}\ \sin(\xi d)}{\mu\xi\ F(\xi)}\ \{\ (k_\beta^2-2\xi^2)\ e^{-x(\xi^2-k_\beta^2)^{1/2}} + 2\xi^2\ e^{-x(\xi^2-k_\alpha^2)^{1/2}}\ \}, \quad (E.1)$$

$$\text{where } F(\xi) = (2\xi^2-k_\beta^2)2 - 4\xi^2\ (\xi^2-k_\alpha^2)^{1/2}\ (\xi^2-k_\beta^2)^{1/2} \quad (E.2)$$

We recover the displacement w(x,z) inverting the Fourier transform (E.1),

$$w(x,z) = 1/(2\pi) \int_R w_F(x,\xi)\ e^{i\xi z}\ d\xi. \quad (E.3)$$

Since $w_F(x,-\xi) = w_F(x,\xi)$ we get in (E.3),

$$w(x,z) = 1/\pi \int_0^\infty w_F(x,\xi)\ \cos(\xi z)\ d\xi. \quad (E.4)$$

We compute w(x=0,z) and take the mean value along DD

$$\langle w\rangle = 1/DD \int_{-d}^{d} w(0,z)\ dz\ . \quad (E.5)$$

Appendix F

NUMERICAL DETAILS

To compute the two integrals (4.2) and (5.2), an adequate change of variable is done; set $\xi = k_\alpha \zeta$, and from $\gamma^2 = k_\beta^2 / k_\alpha^2$ we get $k = k_\alpha (\gamma^2-\zeta^2)^{1/2}$ and $h = k_\alpha (1-\zeta^2)^{1/2}$.

This transformation is useful in locating and bounding the singular points of the integrand for different values of the Poisson's ratio ν.

We limit our interest in the following values of ν:

$$0 < \nu < 0.475 ,$$

this interval gives for γ:

$$\sqrt{2} < \gamma < \sqrt{21} ,$$

since $\gamma^2 = 2(1-\nu)/(1-2\nu)$.

AXICYLIN:

Computation of the Hankel functions H_n is done using the following relation (n=0,1) $x \in R$

$H_n(x) = J_n(x) + Y_n(x)$ for real arguments (ex: $\zeta < 1$)

$H_0(ix) = -2i/\pi\ K_0(x)$ for pure imaginary arguments

$H_1(ix) = -2/\pi\ K_1(x)$ (ex: $\zeta > \gamma$).

where J_n and Y_n are the usual Bessel functions of order n, K_n the modified Bessel function of order n computed using IMSL mathematical library in single precision.

Singularities occurs in the calculation of (4.2) for h=0 or k=0 (i.e. when the argument of the Hankel function vanishes). It can be shown analitically, that for the range of cylinder radius (a < 1m) and for the frequency upper limit 300 Hz,

the contribution in the integral due to the limiting value of the integrand when h=0 (ζ=1) or when k=0 (ζ=γ) is either continuous with its surrounding values (when k or h close to zero) or else the area concerned with the singularity is negligible (case ζ=1 for w^t). Numerical computation has been undertaken to check carefully the analytical results of these singularities. We shall therefore voluntarily skip them in the calculation.

An asymptotic expansion for large arguments of H_n is implemented. The convergence test has been checked and shown to be satisfactory.

Computation of (4.2) done with an IBM 370/168 for a frequency sampling of 4Hz (limit 300Hz) takes about one minute of CPU time.

INFISTRIP:

The presence of the Rayleigh function $F(\zeta) = (2\zeta^2-\gamma^2)^2 - 4\zeta^2 (\zeta^2-1^2)^{1/2} (\zeta^2-\gamma^2)^{1/2}$ in the denominator of (5.2) leads us to consider a complex modulus of rigidity $\mu = \mu_0(1+i\varepsilon)$. By doing so, the Rayleigh pole is shifted upwards from the real axis in the complex plane, and the integration can be performed. The contribution due to the pole is considered when ε is close to zero. A satisfactory value is ε=0.01. The pole ζ_0 is bounded: $\gamma < \zeta_0 < 1.2\ \gamma$. In this interval the integrand is much more closely sampled.

An asymptotic expansion for large values of ζ is implemented. The convergence test is similar to Axicylin's.

Computation of (5.2) with the same frequency spacing and on the same computer takes about 26 seconds of CPU time.

Appendix G

Infistrip, particular case of Axicylin

Let us first see that $-ik = (\xi^2 - k_\beta^2)^{1/2}$ (G.1)

and that the Rayleigh function ,

$$F(\xi) = (2\xi^2 - k_\beta^2)2 - 4\xi^2 (\xi^2 - k_\alpha^2)^{1/2} (\xi^2 - k_\beta^2)^{1/2} \quad \text{(G.2)}$$

$$= (2\xi^2 - k_\beta^2)2 + 4\xi^2 hk \quad \text{(G.2)}$$

Furthermore $H_0(ha)\ H_0(ka) \underset{a \to \infty}{\sim} -2i \dfrac{e^{ia(k+h)}}{\pi a\sqrt{hk}}$. (G.3)

Let us show that when $a \to \infty$, Axicylin would be equivalent to Infistrip:

$$R(\xi) \sim -2 \frac{e^{ia(k+h)}}{\pi a\sqrt{hk}} F(\xi) \quad \text{(see below D.17)} \quad \text{(G.4)}$$

$$A_0(\xi) \sim \frac{2is\ k\ H_o(ka)\ \sin(\xi d)}{\pi \mu\ R(\xi)}$$

$$C_0(\xi) \sim \frac{s(2\xi^2 - k_\beta^2)\ H_o(ha)\ \sin(\xi d)}{\pi \xi \mu k\ R(\xi)}$$

Hence (4.2) reduces to

$$\langle w^t \rangle = \frac{2s}{\pi\mu} \int_0^\infty \frac{H_0(ha)\, H_0(ka)}{R(\xi)} \frac{\sin^2(\xi d)}{\xi^2 d} \{-2\xi^2+k(2\xi^2-k_\beta{}^2)\}\, d\xi,$$

and using the relations (G.2), (G.3) and (G.4) we get

$$\langle w^t \rangle = \frac{2s}{\pi\mu} \int_0^\infty \frac{-ik\, k_\beta{}^2}{F(\xi)} \frac{\sin^2(\xi d)}{\xi^2 d}\, d\xi \quad ,$$

and with (G.1) and DD=2d,

$$\langle w^t \rangle = \frac{s\ DD}{\pi\mu} \int_0^\infty \frac{k_\beta{}^2(\xi^2-k_\beta{}^2)^{1/2}}{F(\xi)} \frac{\sin^2(\xi d)}{(\xi d)^2}\, d\xi$$

which is exactly (5.2).

Appendix H

Solution of the Inhomogeneous Diffusion equation (2.7)

Let us take the Laplace transform of (2.7). Set

$$P(x,s) = \int_0^\infty e^{-st} p(x,t)dt$$

$$Q(s) = \int_0^\infty e^{-st}\, q(t)dt$$

we obtain

$$a^2 \frac{d^2P(x,s)}{dx^2} - s\, P(x,s) = Q(s) - P_o \qquad \text{(H-1)}$$

since $p(x,o) = P_o$.

The general solution to the homogeneous equation of (H-1) is

$$p^H(x,s) = A(S)\exp(-\sqrt{s}\,\frac{x}{a}) + B(s)\exp(\sqrt{s}\,\frac{x}{a})$$

A particular solution of (H-1) is found by searching for a solution of the form $P_{ps}(s)$ only, this results in

$$P_{ps}(s) = \frac{P_o - Q(s)}{s}$$

The general solution of (H-1) is then

$$P(x,s) = P^H(x,s) + P_{ps}(s) \qquad \text{(H-2)}$$

the boundary condition $\frac{\partial p}{\partial x}\Big|_{x=\infty} = 0$ gives

$$\frac{\partial P}{\partial x}\Big|_{x=\infty} = 0 \rightarrow B(s) = 0.$$

$p(o,t) = P_o \rightarrow P(o,s) = P_o/s$ so that $A(s) = \frac{Q(s)}{s}$.

The general solution of (H-1) satisfying the boundary condition is then

$$P(x,s) = -\frac{Q(s)}{s}\left(\frac{1-\exp(-\sqrt{s}\,\frac{x}{a})}{s}\right) + \frac{P_o}{s} \qquad \text{(H-3)}$$

Inverting in the time domain (H-3) and recalling that

$$\frac{1-\exp(-k\sqrt{s})}{s} \rightarrow \operatorname{erf}\left(\frac{k}{2\sqrt{t}}\right),$$

$$Q(s).G(s) \rightarrow \int_o^t q(\tau)g(t-\tau)d\tau = \int_o^t q(t-\tau)g(\tau)d\tau,$$

we get

$$p(x,t) = P_o - \int_o^t q(t-\tau)\operatorname{erf}\left(\frac{x}{2a\sqrt{\tau}}\right)d\tau \qquad \text{(H-4)}.$$

Appendix I

3D Extrapolation

The stationary solution for an incompressible viscous fluid enclosed between two parallel planes distant of L is for the following boundary conditions: at $x=R$ $p=P_o$ and at $x=R+d$ $p=P_f$

$$p_{2D} = \frac{P_f - P_o}{d} (x - R) + P_o. \qquad (I.1)$$

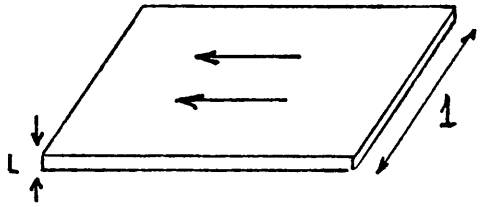

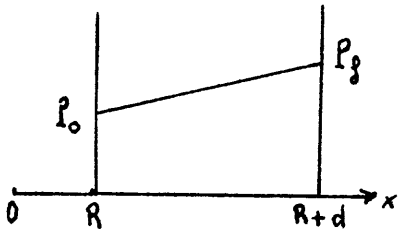

Consider the 3D problem of two discs distant of L with radial flow into the center. The outer radius is $r=R+d$ and the inner radius $r=R$. The boundary conditions are at $r=R$ $p=P_o$ and at $r=R+d$ $p=P_f$. The stationary solution for the pressure distribution is:

$$p_{3D} = \frac{P_f - P_o}{\ln\left(\frac{R+d}{R}\right)} \ln (r/R) + P_o . \qquad (I.2)$$

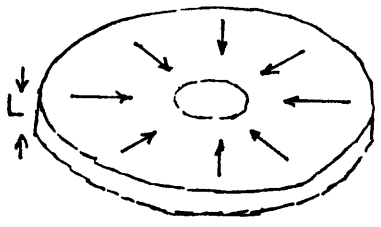

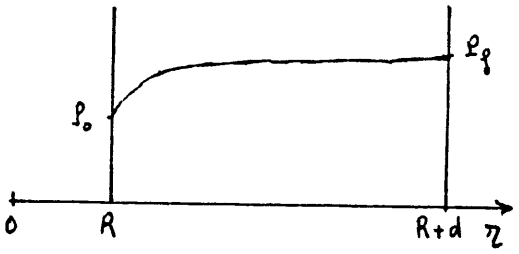

The rate of flow for these two problems is

$$q_{2D} = KL/\eta \quad dp_{2D}/dx$$

$$q_{3D} = KL/\eta \quad 2\pi r \, dp_{3D}/dr \quad ,$$

or explicitly at r=R

$$q_{2D} = KL/\eta \, (P_f - P_o)/d \tag{I.3}$$

$$q_{3D} = KL/\eta \, (P_f - P_o) \, \frac{2\pi}{\ln\left(\frac{R+d}{R}\right)} \, . \tag{I.4}$$

Combining these two results we obtain:

$$q_{3D} = 2\pi R \, \chi \, q_{2D} \tag{I.5}$$

where $\chi = \frac{d/R}{\ln\left(\frac{R+d}{R}\right)}$.

χ is defined as the geometrical factor. For $d \ll R$ we have $\chi \sim 1$. The equation for the volumes is similar to (I.5)

$$\Delta V_{3D} = 2\pi R \, \chi \quad \Delta V_{2D} \, . \tag{I.6}$$

Extending this result to our problem is consistent, since we are in the low frequency approximation. d would be the effective distance defined as the maximum distance that a fluid particle would travel to reach the borehole in T/4. Since the particle velocity in the fluid is lower than the sound velocity in the fluid α_f (subsonic flow)

we therefore have a relation between d and the period T.

d = vel. x $T/4 = E\ \alpha_f\ T/4$ where $E < 1$.

We obtain d= 375 ET (m). We shall choose a reasonable value for A to be 0.1 so that d=37.5 T (m).

All the numbers in table 3, 4 and 5 can be adapted to the present 3D extrapolation of a circular fracture by multiplying them by the factor $\pi\chi/2$. Table 6. gives some results for a "sediment".

Table 6.
("Sediment")

f (Hz)	d (m)	χ	$\lvert u_z^T \rvert / \varepsilon_o L_o$ at $r=R^+$ (m^{-1})
200	0.187	1.8	5116
100	0.375	2.4	2981
50	0.75	3.5	1852
25	1.5	5.4	1188
10	3.75	10.3	711

Appendix J

Tube Wave Formulation

The tube wave displacement field $\underset{\sim}{u}^T$ in the fluid borehole and in the elastic homogeneous medium external to the borehole can be given in terms of the scalar potentials ϕ and ψ representing P and SV waves respectively. No SH-waves exist if we assume axisymmetry. We have

$$\underset{\sim}{u}^T = \nabla\phi + \nabla x(o, \psi, o) \qquad (J.1)$$

Cheng and Toksoz (1981) give the following potentials for guided or interface waves.

(i) In the fluid:

$$\phi_f = C\ I_o(nr)\sin k(z-ct) \qquad r<R^- \qquad (J.2)$$

$$\psi_f = 0 \ ,$$

where $n = k(1 - c^2/\alpha_f^2)^{1/2}$

$$|u^T_{fz}| = k\ C\ I_o(nr) \qquad (J.3)$$

(ii) In the formation:

$$\phi = A\ K_o(\ell r)\sin k(z-ct) \qquad r>R^+$$

$$\psi = B\ K_1(mr)\sin k(z-ct) \ ,$$

where $\ell = k(1-c^2/\alpha^2)^{1/2}$

$m = k(1 - c^2/\beta^2)^{1/2}$.

A and B are related by the boundary condition that the shear stress vanishes at the borehole boundary r=R.

$$|u_z^T| = A[kK_o(\ell r)+mGK_o(mr)] \qquad (J.4)$$

where $$G = \frac{2\ell V_s^2 K_1(\ell R)}{k(c^2-2V_s^2)K_1(mR)}$$

Applying the continuity of radial displacement and stress at r=R, we obtain the period equation that governs the dispersion characteristics of the guided waves.

We have

$$C = \frac{\ell c^2 K_1(\ell R)}{n(2V_s^2-c^2)I_1(nR)} \cdot A$$

The volumetric strain in the fluid is given by

$$\varepsilon_{ii} = \nabla \cdot \underset{\sim}{u}_f^T = \nabla^2 \phi_f$$

integrated over the borehole radius and during T/4 gives at z=o:

$$\Delta V_{3D} = 2\pi c \int_o^R \int_o^{T/4} \nabla^2 \phi_f \, r dr dt \qquad (J.5)$$

From (J.2), use of the Laplacian in cylindrical coordinates gives

$$\nabla^2 \phi_f = C\, k^2 \left(\frac{c^2}{\alpha_f^2} - 2\right) I_o(nr) \sin k(z-ct)$$

Recalling that $\int_o^R I_o(nr) r dr = \frac{R}{n} I_1(nR)$, we get from (J.5)

$$\Delta V_{3D} = C \frac{2\pi R(2-c^2/\alpha^2 f)}{(1-c^2/\alpha_f^2)^{1/2}} I_1(nR).$$

References

Data and references at Schlumberger in Paris (Clamart) were used.

Abramowitz, M., Stegun, I.A., 1970, Handbook of Mathematical Functions, Dover Publications Inc., New York,

Aki, K., Richards, P.G., 1980, Quantitative Seismology: Theory and Methods, Vol. 1, W.H. Freeman & Co., San Francisco.

Brace, W.F. and Walsh, J.B. ,1968, Permeability of granite under high pressure, JGR, 73, 2224-2236.

Bycroft, G.N., 1956, Forced vibrations of a rigid circular plate on a semi-infinite elastic space and on an elastic stratum, Phil. Trans. R. Soc. A, 248, 327-368.

Cheng, C.H.; Toksoz, M.N.: 1981, Tube wave propagation and attenuation in a borehole. Preprint.

_____ : 1981, Elastic wave propagation in a fluid-filled borehole and synthetic logs, Geophysics, 46, 1042-1053.

Gladwell, G.M.L., 1968, Forced tangential and rotatory vibration of a rigid circular disc on a semi-infinite solid, Int. J. Engng. Sci., 6, 559-607.

Huang, C., Hunter, J.A., 1981, Correlation of tube wave events with open fractures in fluid-filled boreholes, Geological survey of Canada report.

Jaeger, J.C., Cook, N.G.W., 1979, Fundamentals of Rock Mechanics, Chapman and Hall, London.

Lamer, A., 1968, Couplage sol-geophone, Institut Francais du Petrole, Ref: 16-341.

Lamer, A., 1970, Couplage sol-geophone, Geophys. Prosp., 18, 300-319.

Landau, L.D., Lifshitz, E.M., 1959, Fluid Mechanics, Pergamon Press.

Luco, J.E., Westmann, R.A., 1971, Dynamic response of circular footings, UCLA Eng. 7113.

Mavko, G.M and Nur, A., 1979, Wave attenuation in partially saturated rocks, Geophysics, 44, 161-178.

Miller, G.F., Pursey, H., 1954, The field and radiation impedance of mechanical radiators on the free surface of a semi-infinite isotropic solid, Proc. Roy. Soc. London, Series A223, 521-541.

Safar, M.N., 1978, On the minimization of the distorsion caused by the geophone-ground coupling, Geophys. Prosp., 26, 538-549.

Watson, G.N., 1944, Theory of Bessel Functions, Cambridge Univ. Press.

White, J.E., 1965, Seismic waves, radiation, transmission and attenuation, Mc Graw Hill Book Company.

Figure Captions

Fig. 1 General definition of the coupling

Fig. 2 Tool WST

Fig. 3 Test well X profile

Fig. 4 Selected signals from test well X

Fig. 5 Representative signals in a shale and in a limestone

Fig. 6 Signals of Fig. 5 filtered 10-80 Hz

Fig. 7 Amplitude spectrums of signals of Fig. 5

Fig. 8 Amplitude spectrum in the range 0-120Hz of signals of Fig. 5

Fig. 9 Detailed definition of the coupling

Fig. 10 Approximations concerned with the models Axicylin and Infistrip

Fig. 11 Model Axicylin

Fig. 12 Model Infistrip

Fig. 13 Amplitude spectrum of T for a soft formation (Axicylin) with $\delta = 2$ cm and the WST

Fig. 14 Same as Fig. 13 with $\delta = 4$ cm

Fig. 15 Same as Fig. 13 with $\delta = 6$ cm

Fig. 16 Amplitude spectrum of T for a hard formation (Axicylin) with $\delta = 1$ cm and the WST

Fig. 17 Amplitude spectrum of T for a soft formation (Infistrip) with $\delta = 2$ cm and the WST

Fig. 18 Same as Fig. 17 with $\delta = 4$ cm

Fig. 19 Same as Fig. 17 with $\delta = 6$ cm

Fig. 20 Amplitude spectrum of T for a hard formation (Infistrip) with $\delta = 2$ cm

Fig. 21 Tube wave displacement in a borehole

Fig. 22 2D Fracture model

Fig. 23 Storage of Fluid in fracture

Fig. 24 3D model of strip fracture

Fig. 25 Observation of tube wave generation

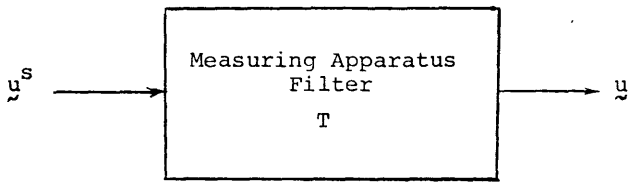

Figure 1.

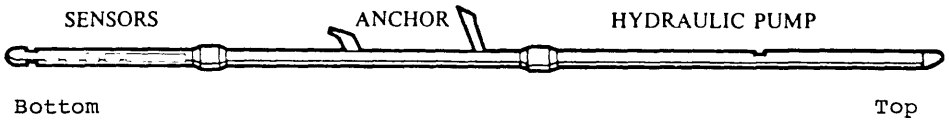

Figure 2.

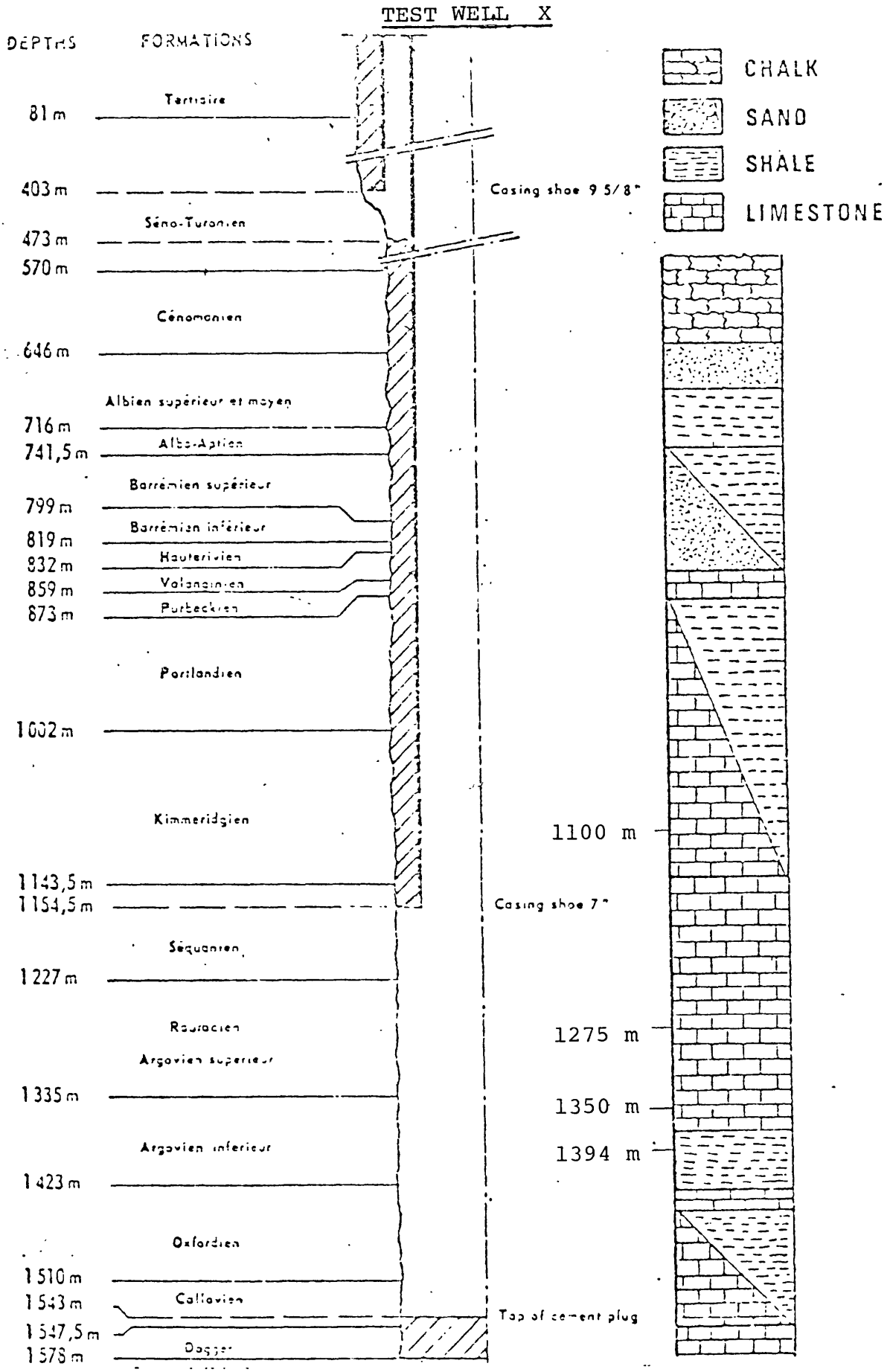
TEST WELL X
DEPTHS
FORMATIONS
81 m
Tertiaire
403 m
Casing shoe 9 5/8"
Séno-Turonien
473 m
570 m
Cénomanien
646 m
Albien supérieur et moyen
716 m
741,5 m
Alb-Aptien
Barrémien supérieur
799 m
Barrémian inférieur
819 m
832 m
Hauterivien
859 m
Valanginien
873 m
Purbeckien
Portlandien
1002 m
Kimmeridgien
1143,5 m
1154,5 m
Casing shoe 7"
Séquanien
1227 m
Rauracien
Argovien supérieur
1335 m
Argovien inferieur
1423 m
Oxfordien
1510 m
1543 m
Callovien
1547,5 m
Dogger
1578 m
Top of cement plug
CHALK
SAND
SHALE
LIMESTONE
1100 m
1275 m
1350 m
1394 m

Figure 3.

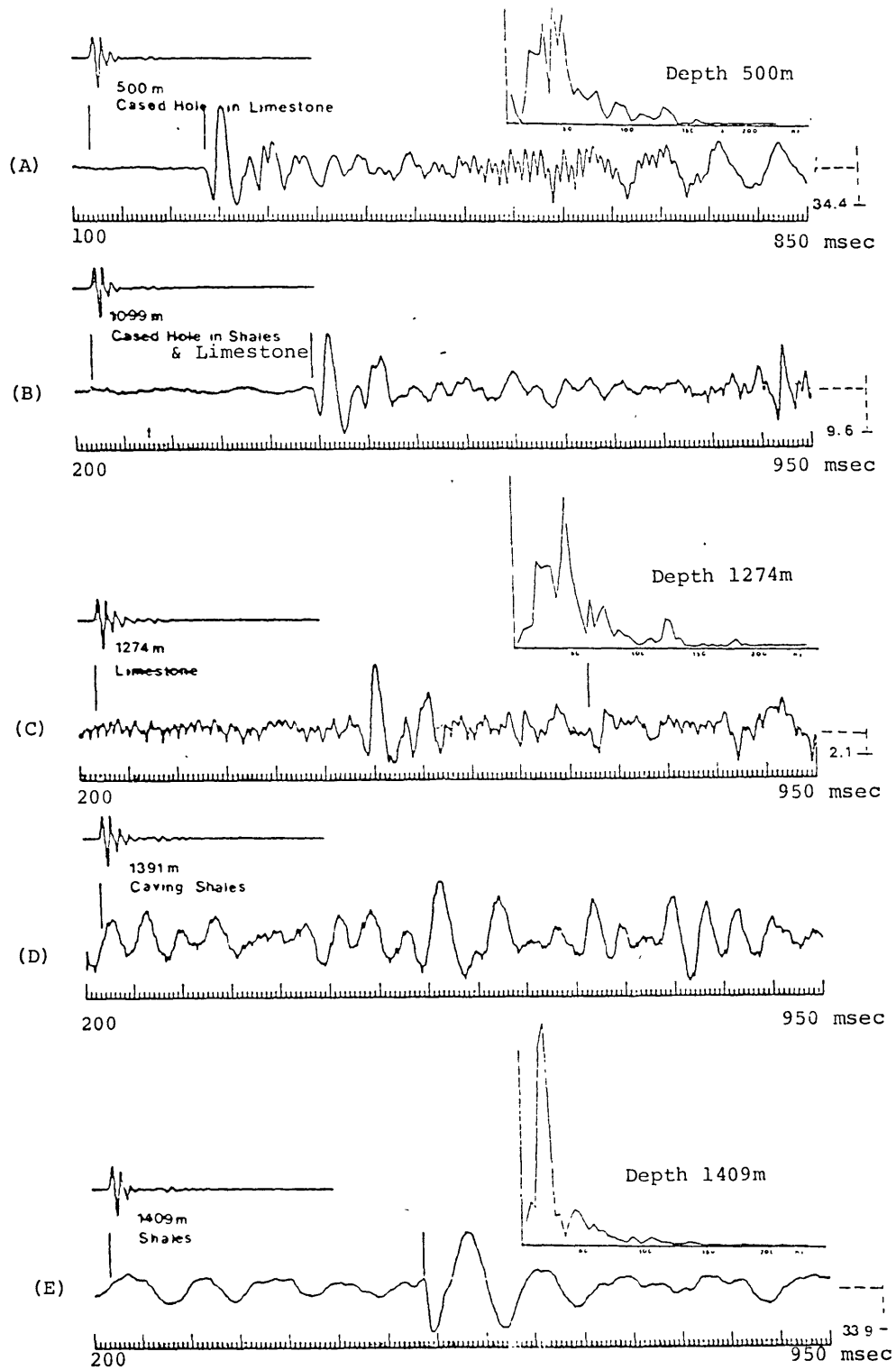
Depth 500m
500 m
Cased Hole in Limestone
(A)
34.4
100
850 msec
1099 m
Cased Hole in Shales
& Limestone
(B)
9.6
200
950 msec
Depth 1274m
1274 m
Limestone
(C)
2.1
200
950 msec
1391 m
Caving Shales
(D)
200
950 msec
Depth 1409m
1409 m
Shales
(E)
33 9
200
950 msec

Figure 4.

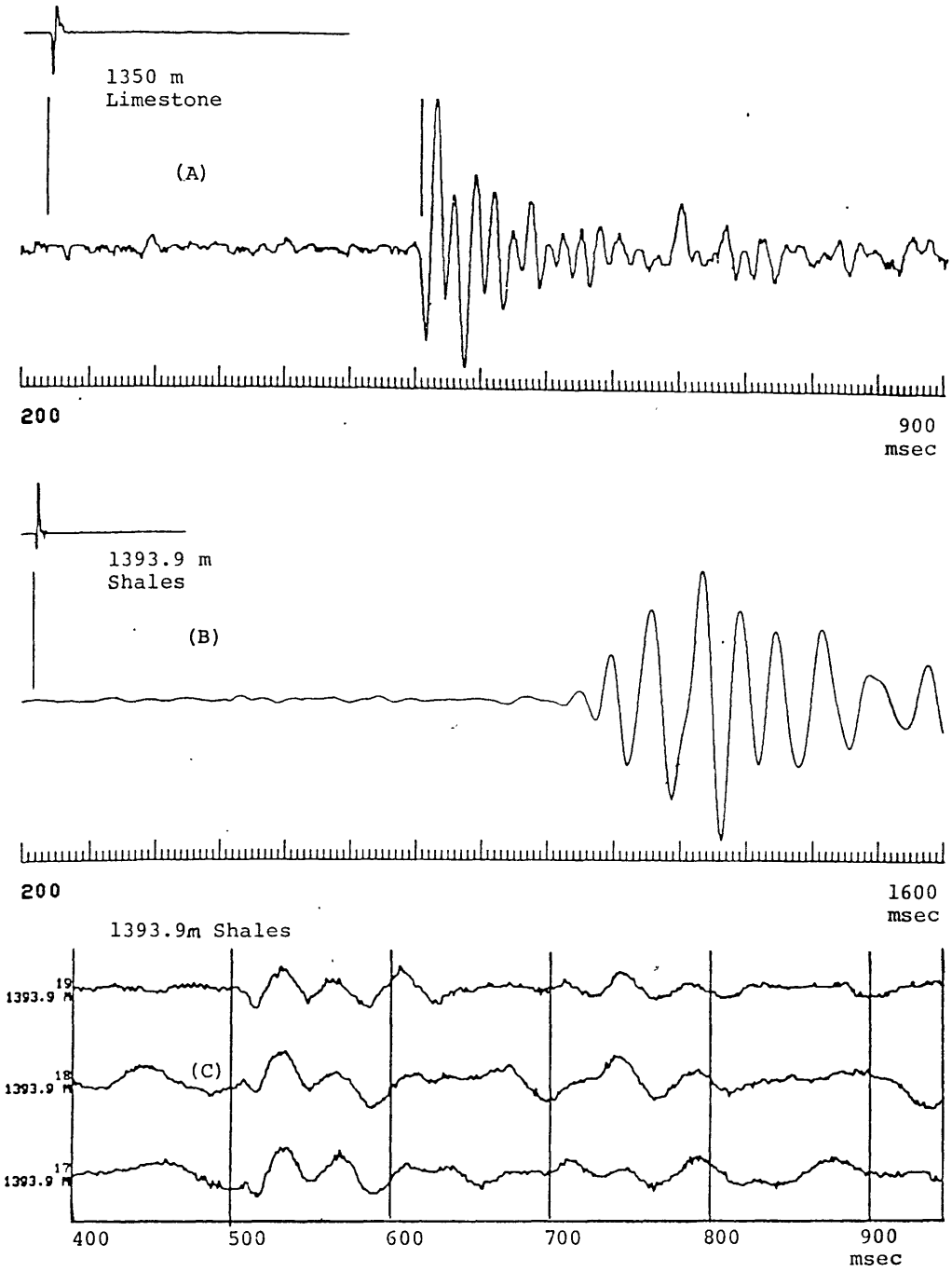
1350 m
Limestone
(A)
200
900
msec
1393.9 m
Shales
(B)
200
1600
msec
1393.9m Shales
1393.9 19 m
1393.9 18 m
(C)
1393.9 17 m
400
500
600
700
800
900
msec

Figure 5.

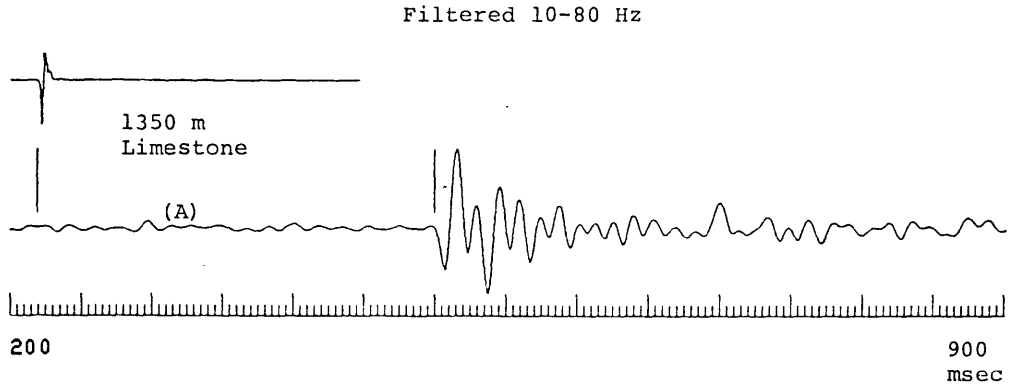
Filtered 10-80 Hz
1350 m
Limestone
(A)
200
900
msec

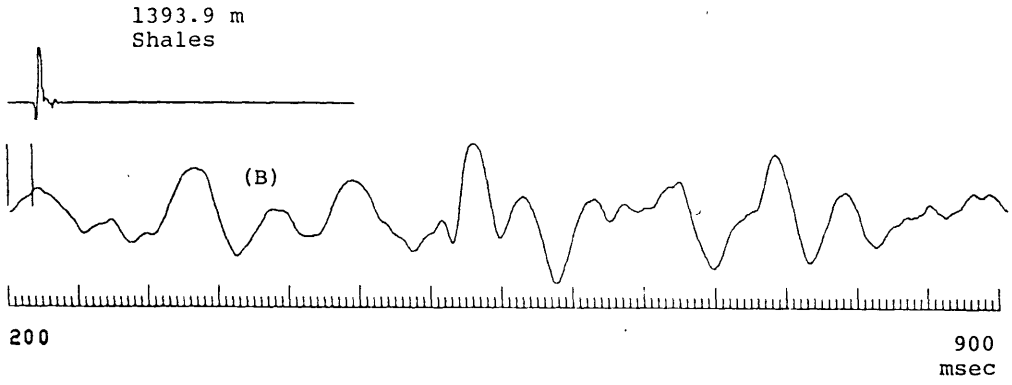
1393.9 m
Shales
(B)
200
900
msec

Figure 6.

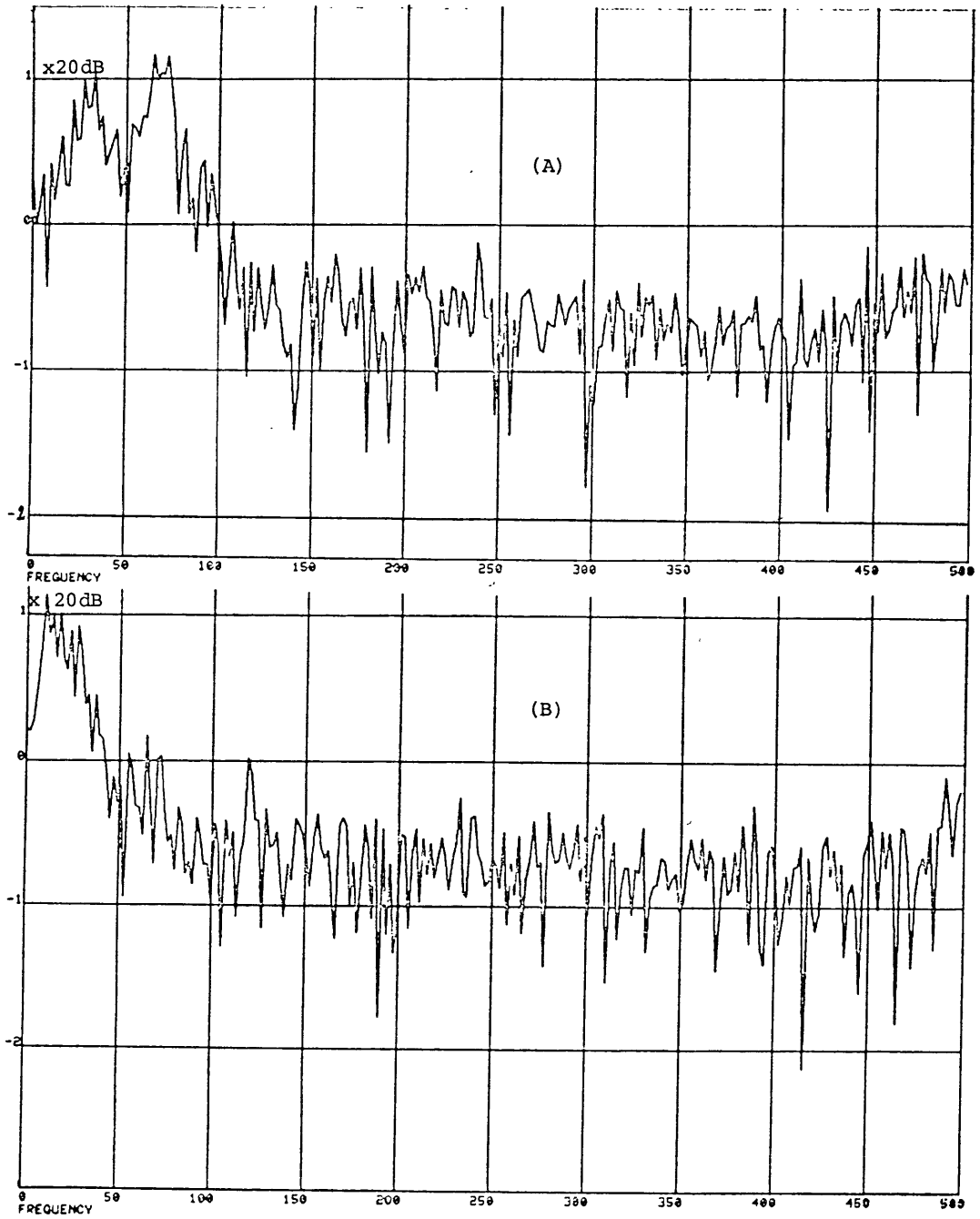
x20dB
(A)
1
0
-1
-2
0
FREQUENCY
50
100
150
200
250
300
350
400
450
500
x20dB
(B)
1
0
-1
-2
0
FREQUENCY
50
100
150
200
250
300
350
400
450
500

Figure 7.

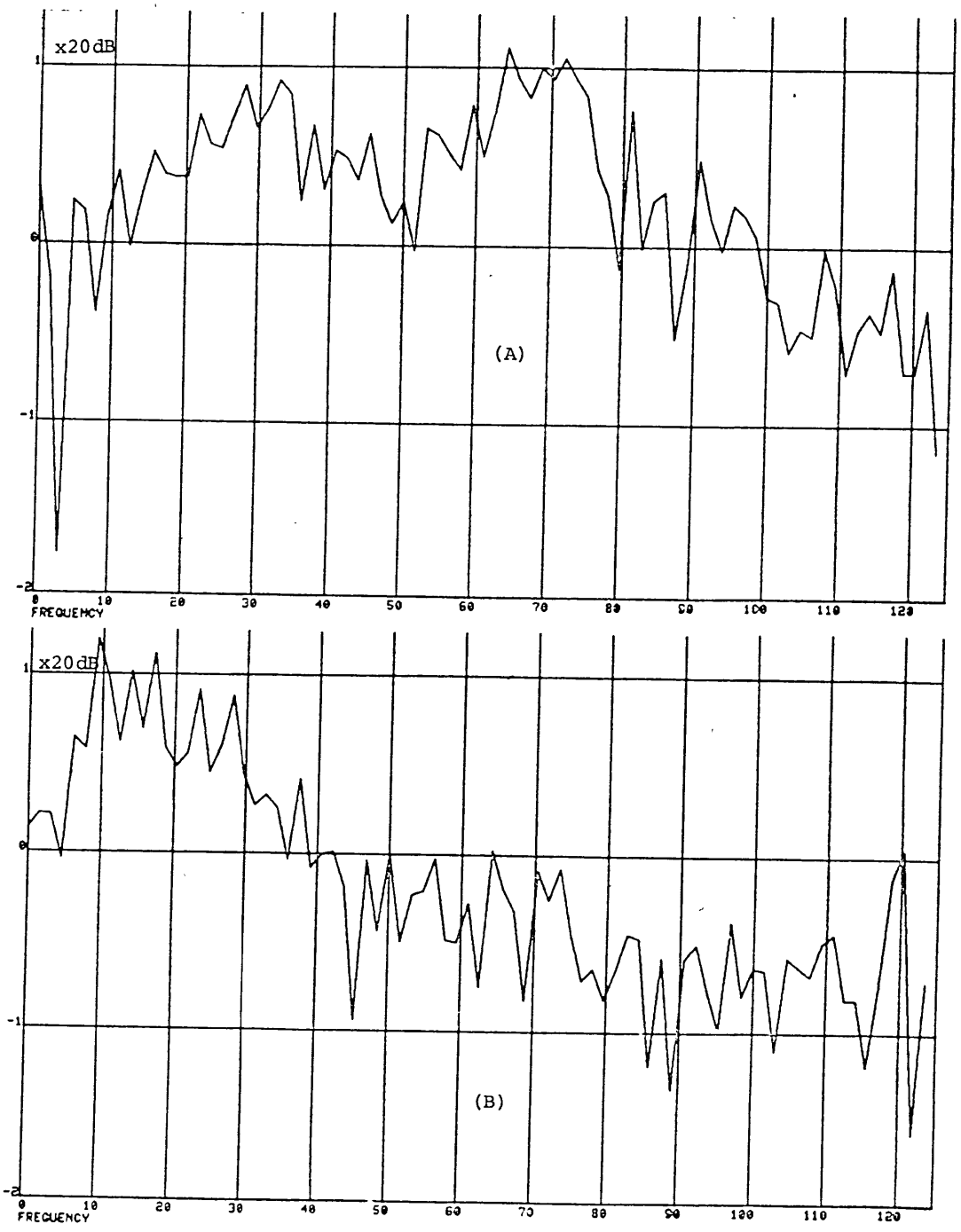
x20dB
1
0
-1
-2
(A)
0 10 20 30 40 50 60 70 80 90 100 110 120
FREQUENCY
x20dB
1
0
-1
-2
(B)
0 10 20 30 40 50 60 70 80 90 100 110 120
FREQUENCY

Figure 8.

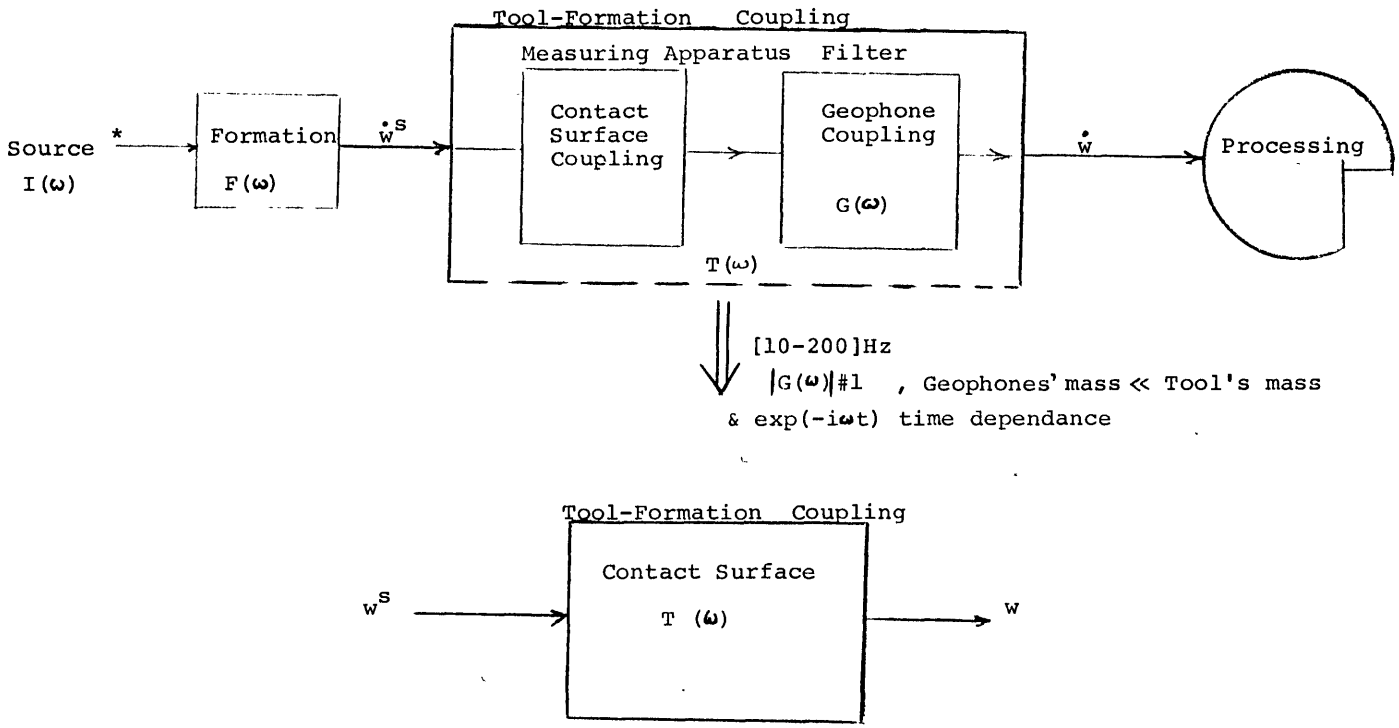
Tool-Formation Coupling
Measuring Apparatus Filter
Source
I(ω)
*
Formation
F(ω)
$\dot{w}^s$
Contact
Surface
Coupling
Geophone
Coupling
G(ω)
$\dot{w}$
Processing
T(ω)
[10-200]Hz
|G(ω)|#1 , Geophones' mass ≪ Tool's mass
& exp(-iωt) time dependance
Tool-Formation Coupling
Contact Surface
T (ω)
w^s
w

Figure 9 .

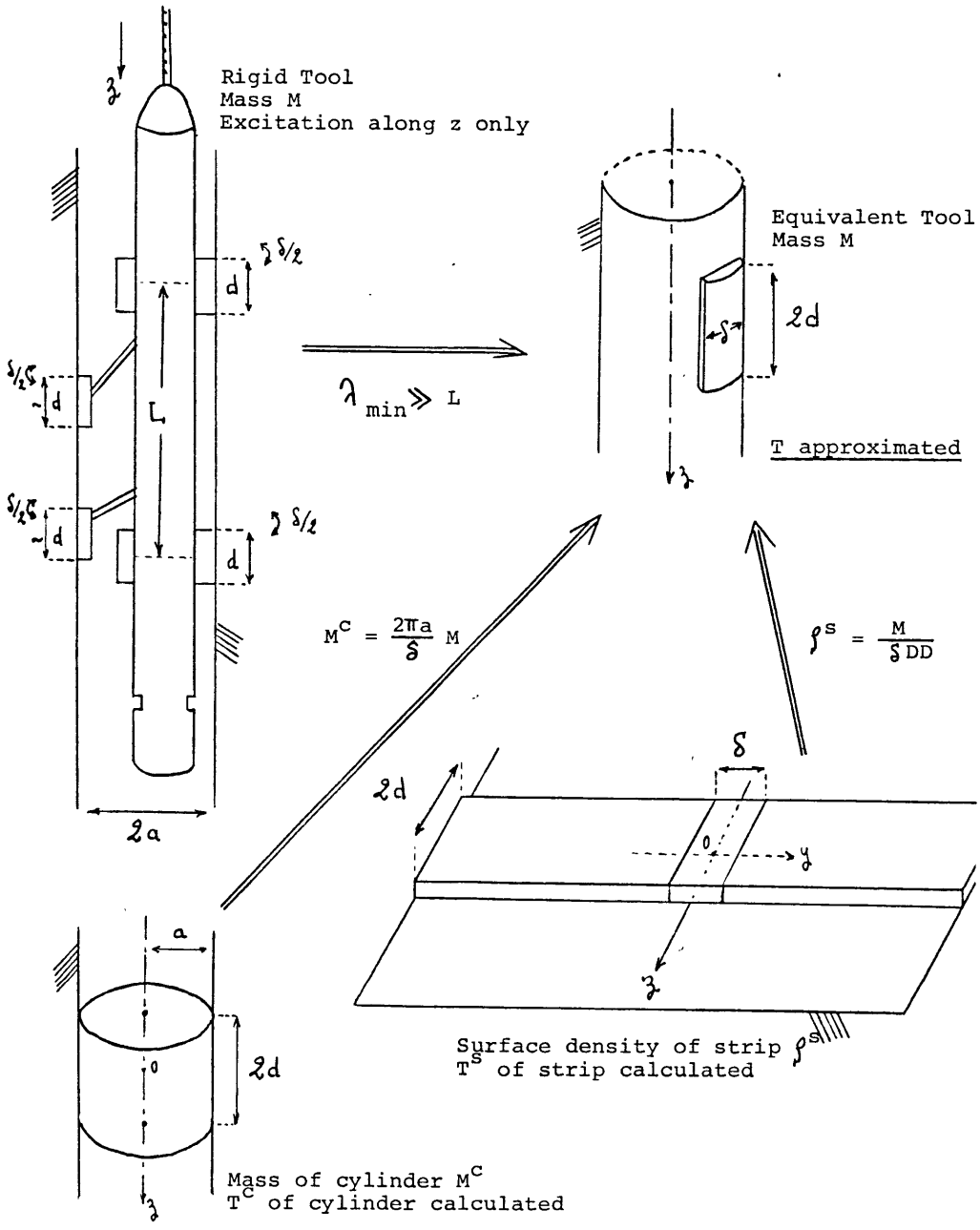
Rigid Tool
Mass M
Excitation along z only
Equivalent Tool
Mass M
T approximated
$\lambda_{min} \gg L$
$M^c = \frac{2\pi a}{\delta} M$
$\rho^s = \frac{M}{\delta DD}$
Surface density of strip ρ^s
T^s of strip calculated
Mass of cylinder M^c
T^c of cylinder calculated
Model Axicylin
Model Infistrip

Figure 10.

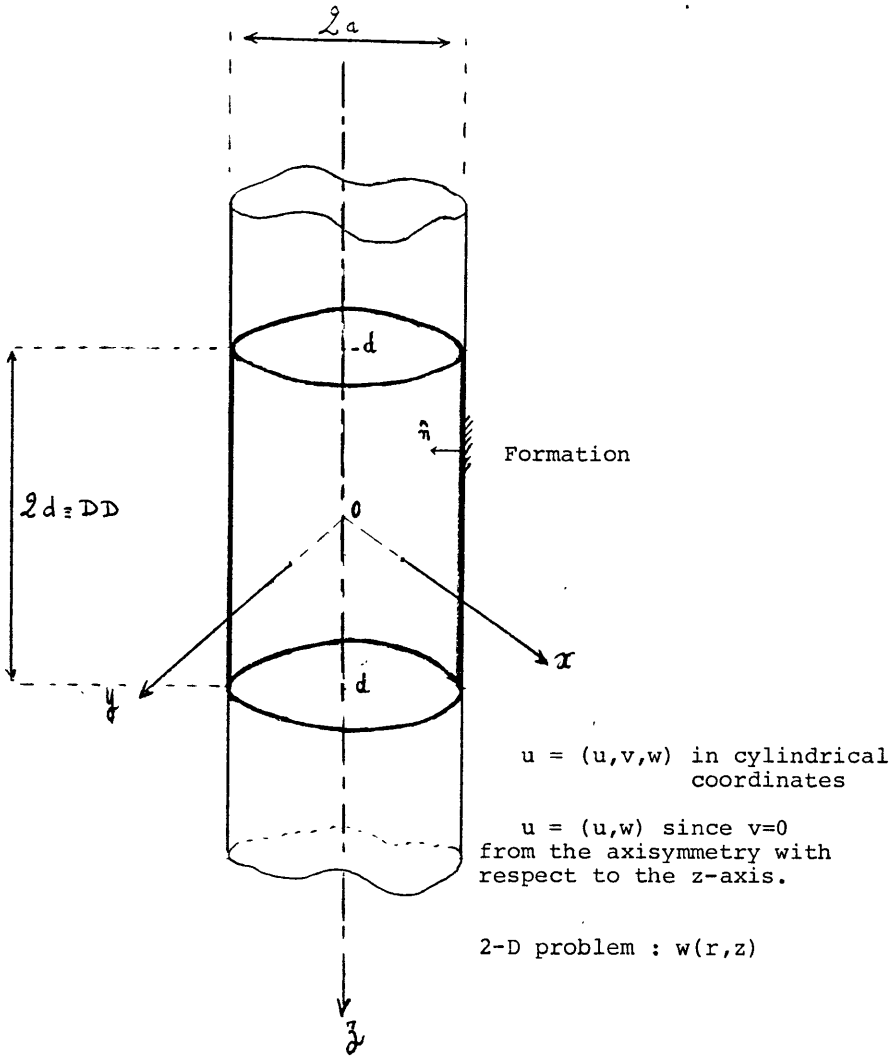
2a
d
n
Formation
2d = DD
0
x
y
d
z
u = (u,v,w) in cylindrical coordinates
u = (u,w) since v=0 from the axisymmetry with respect to the z-axis.
2-D problem : w(r,z)

Figure 11.

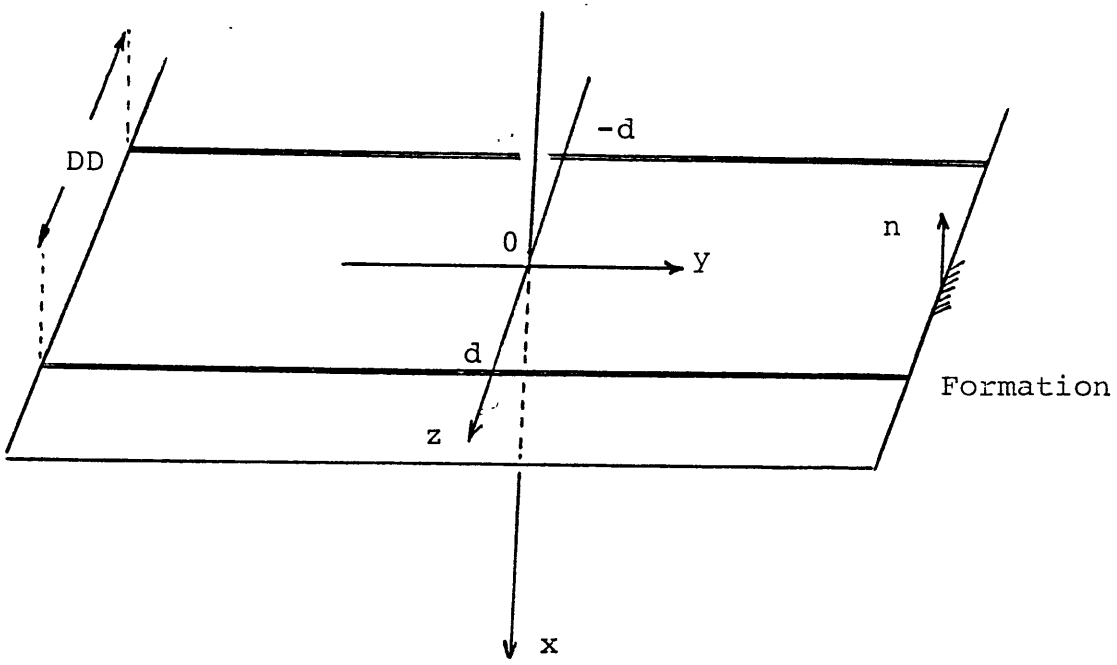

u = (u,v,w) in cartesian coordinates
u = (u,w) since v=0 from the plane symmetry with respect to x0z.
2-D problem : w(x,z)

Figure 12.

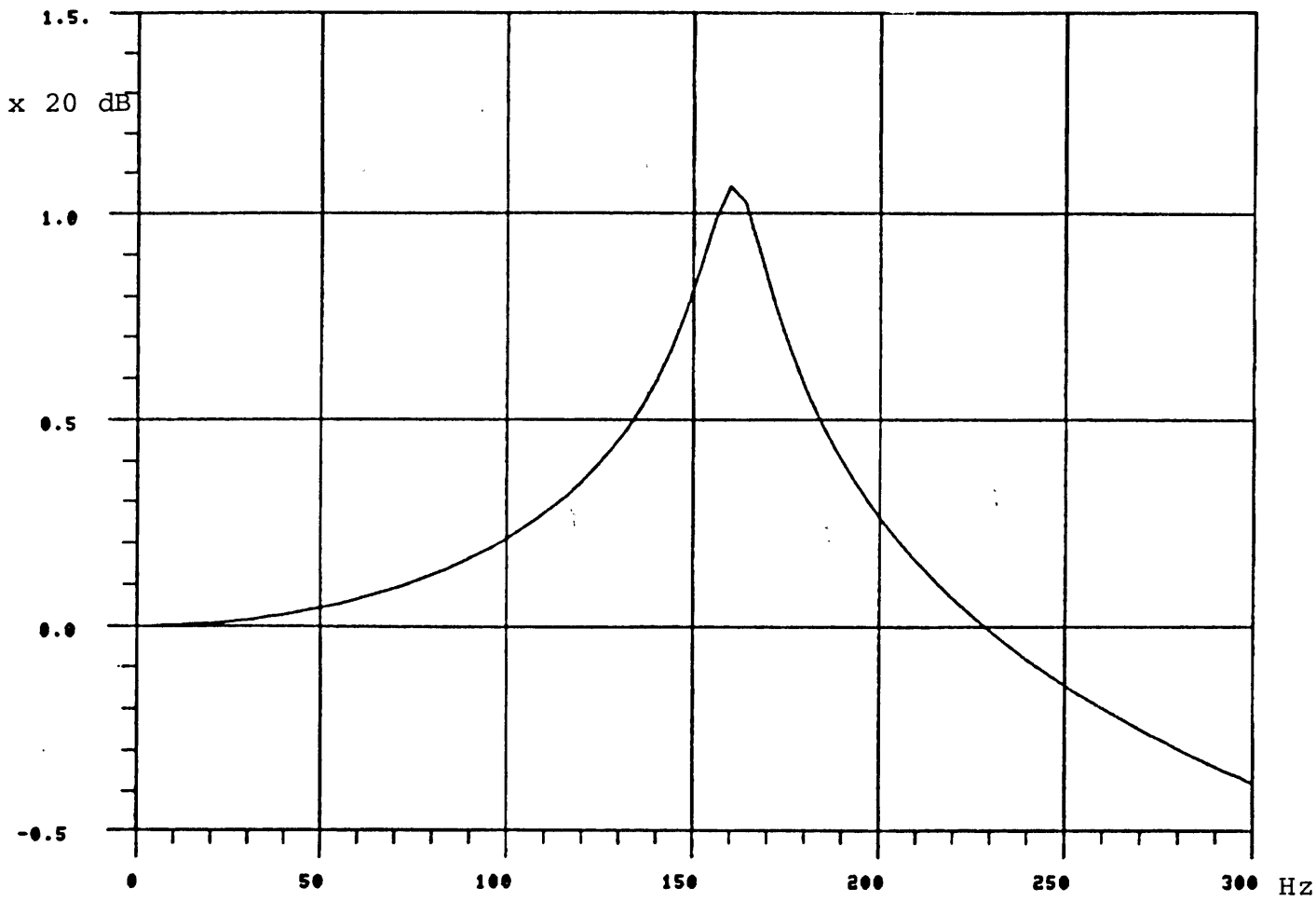

Figure 13.

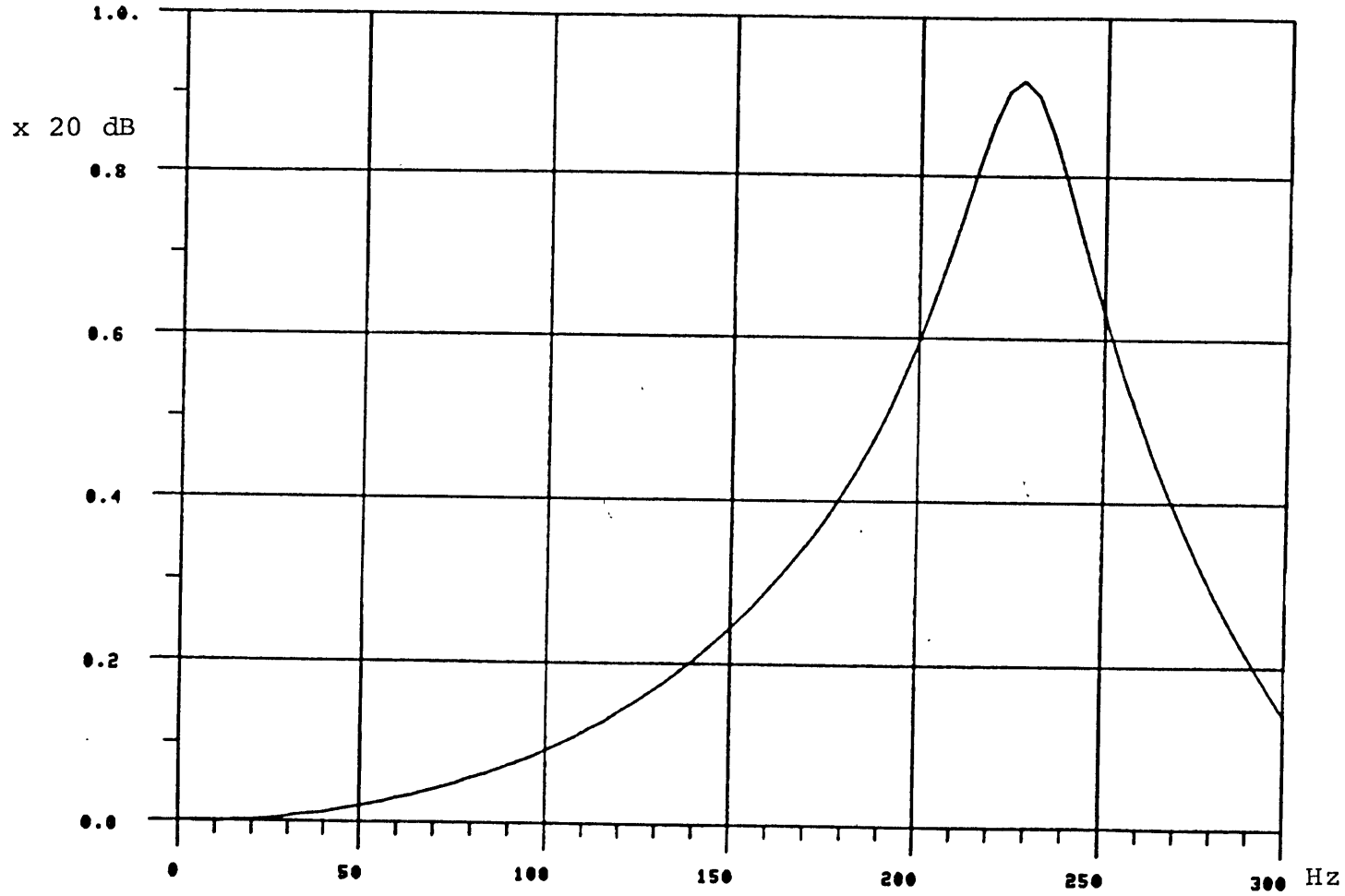

Figure 14.

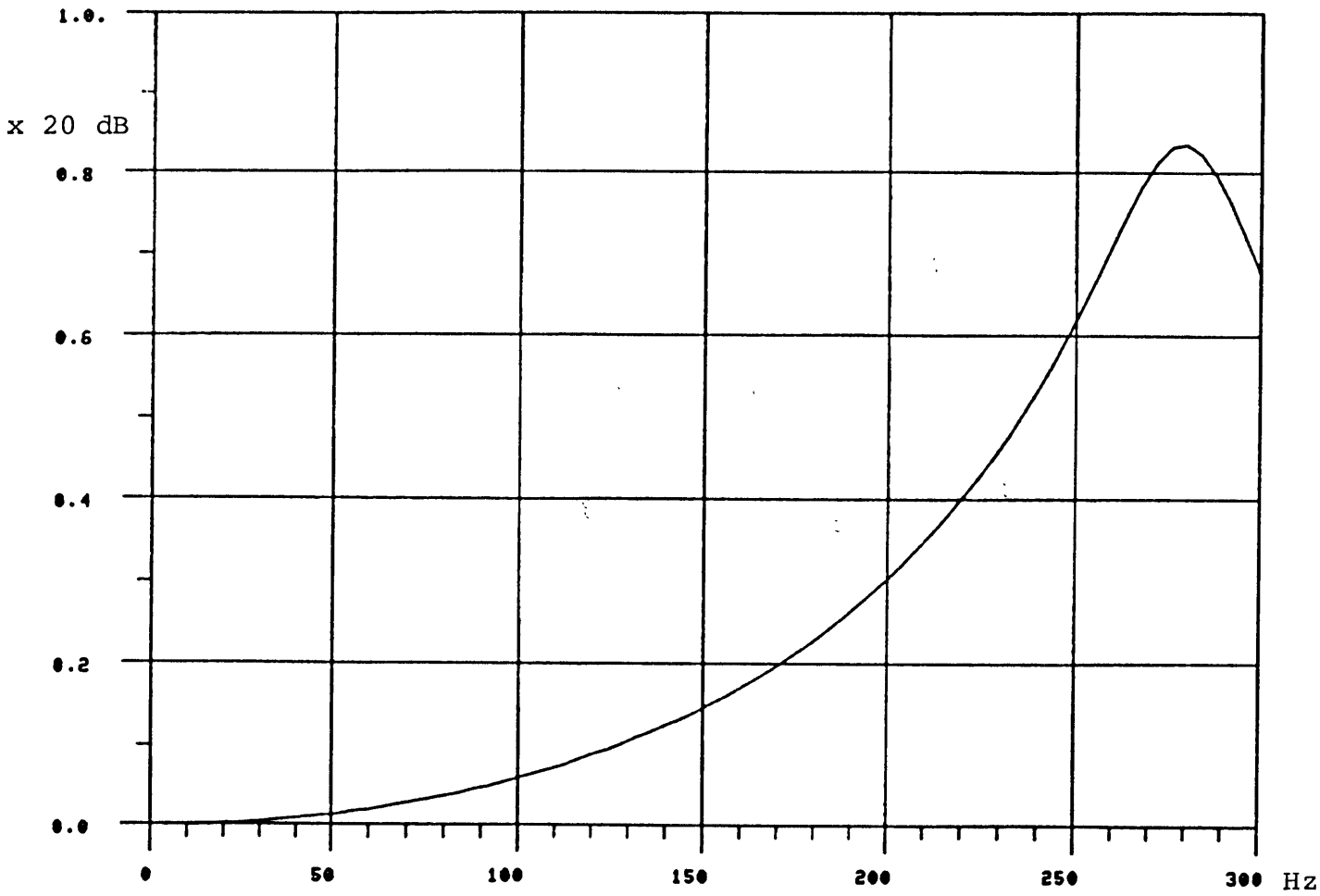

Figure 15.

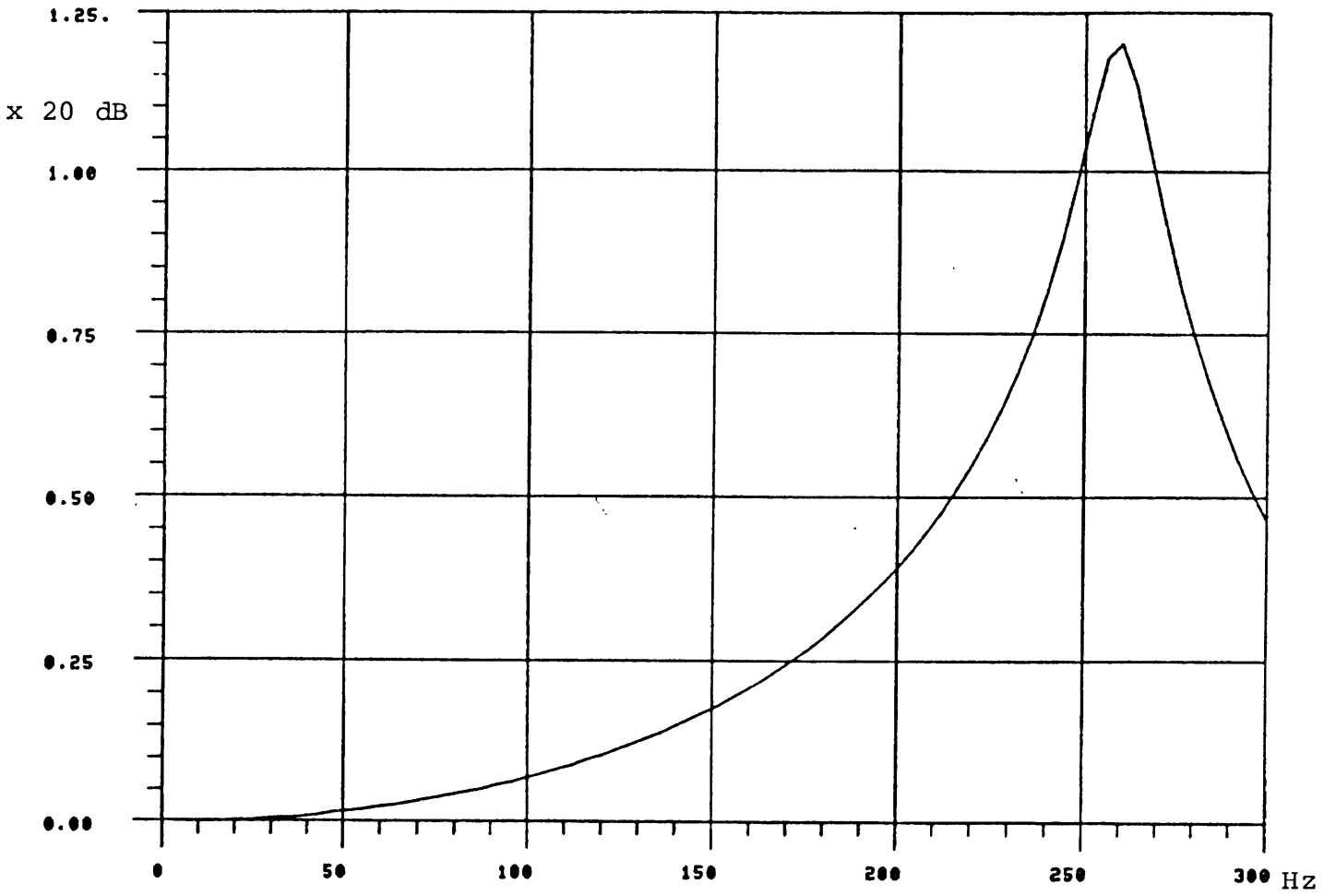

Figure 16.

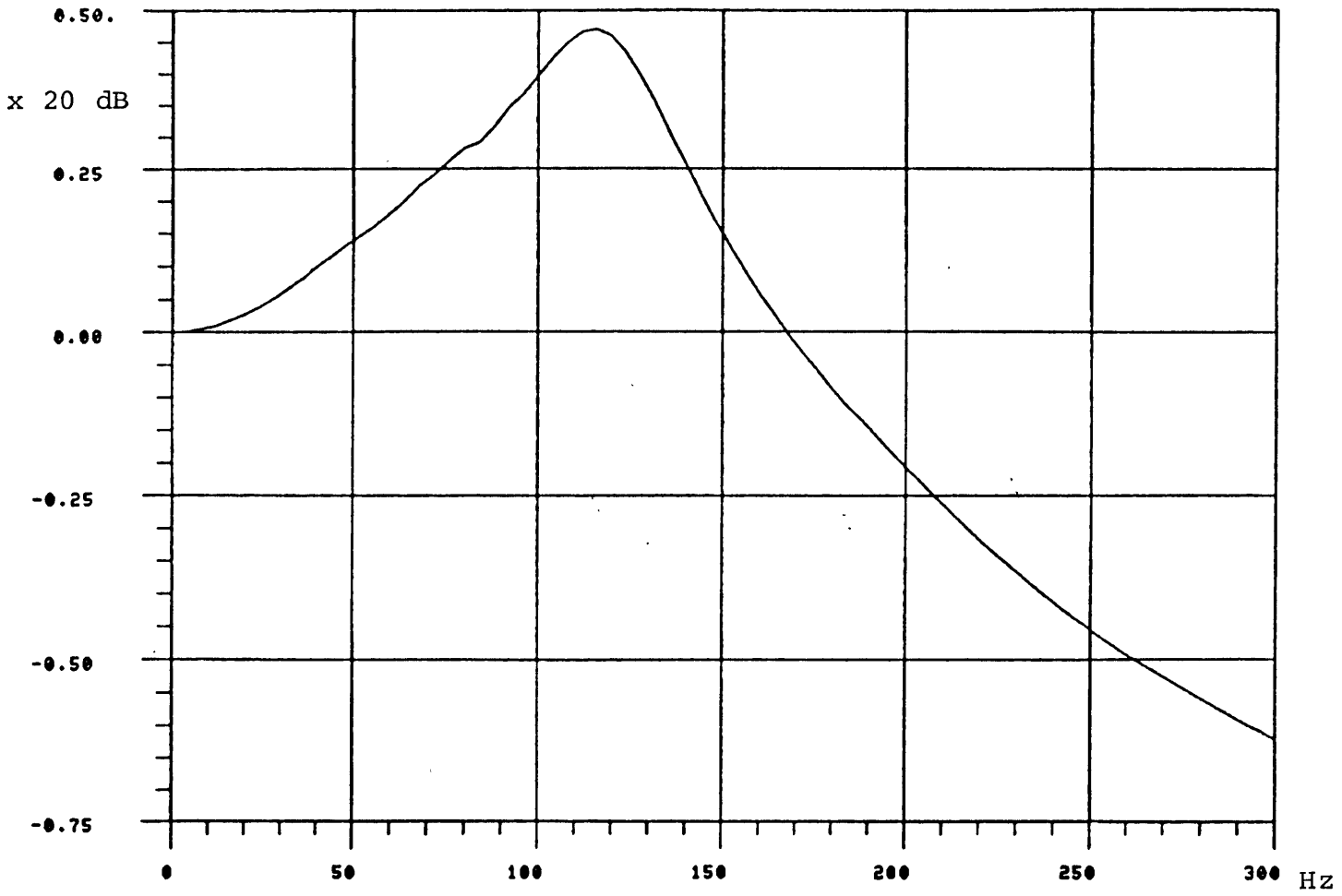

Figure 17.

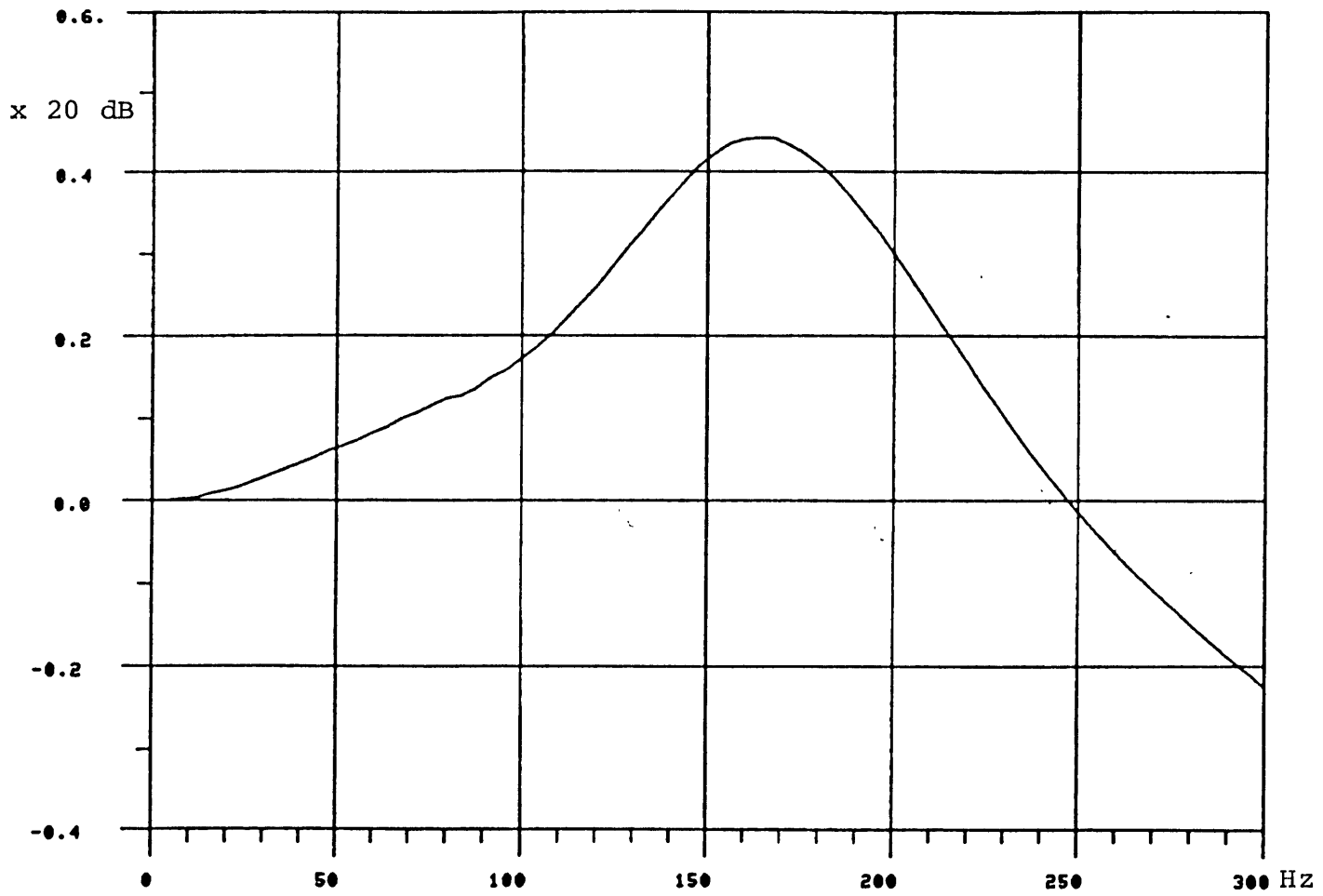

Figure 18.

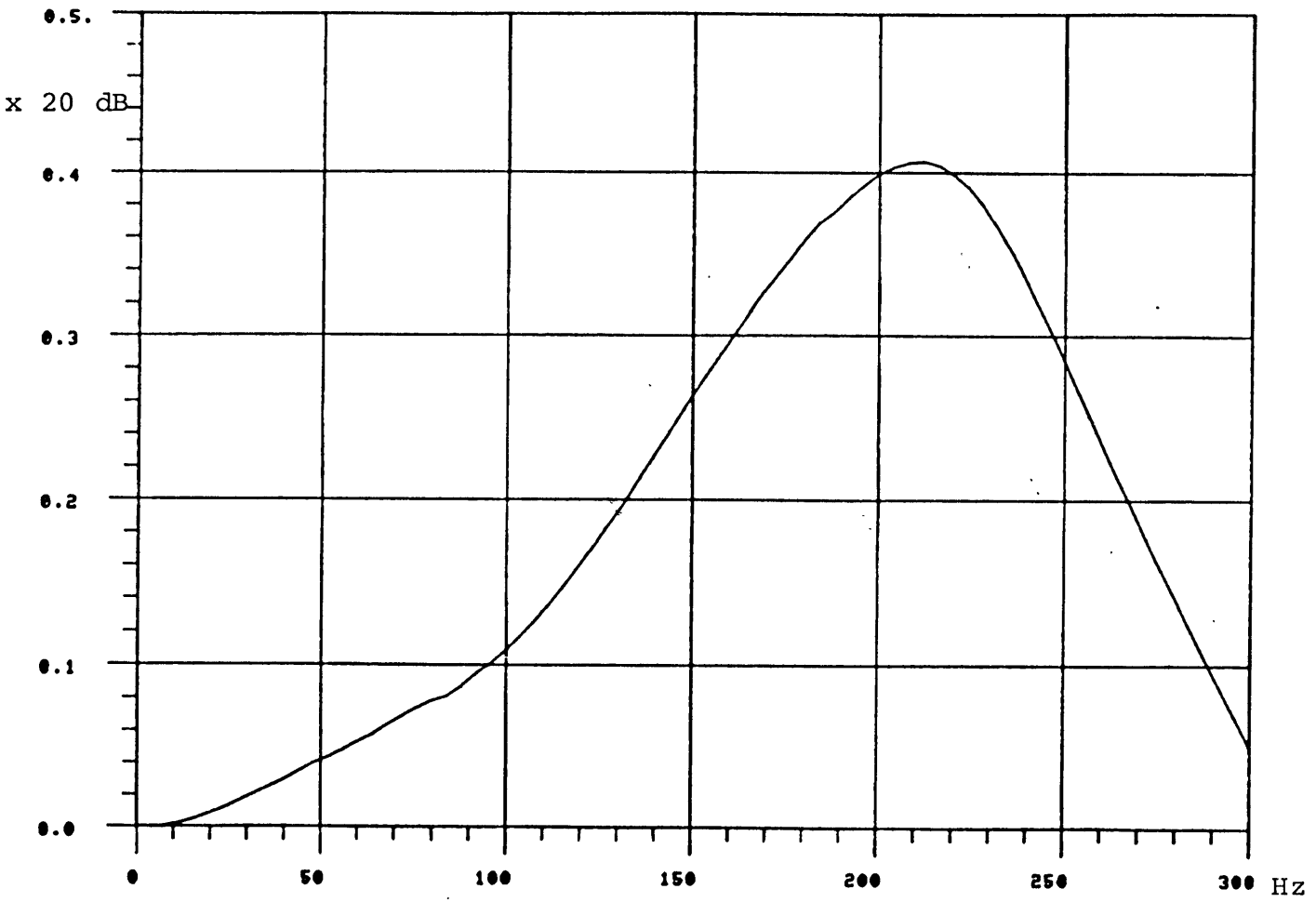

Figure 19.

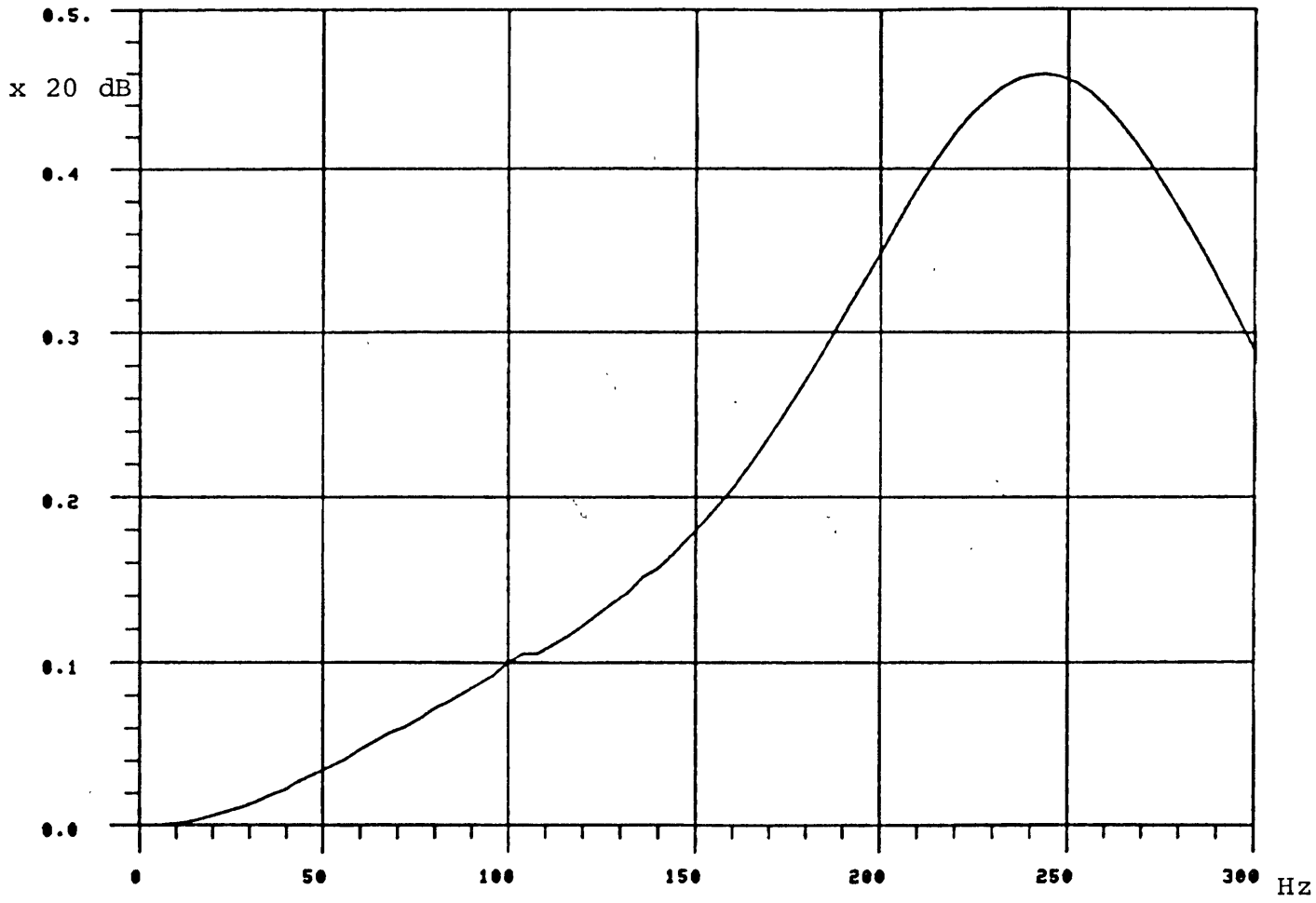

Figure 20.

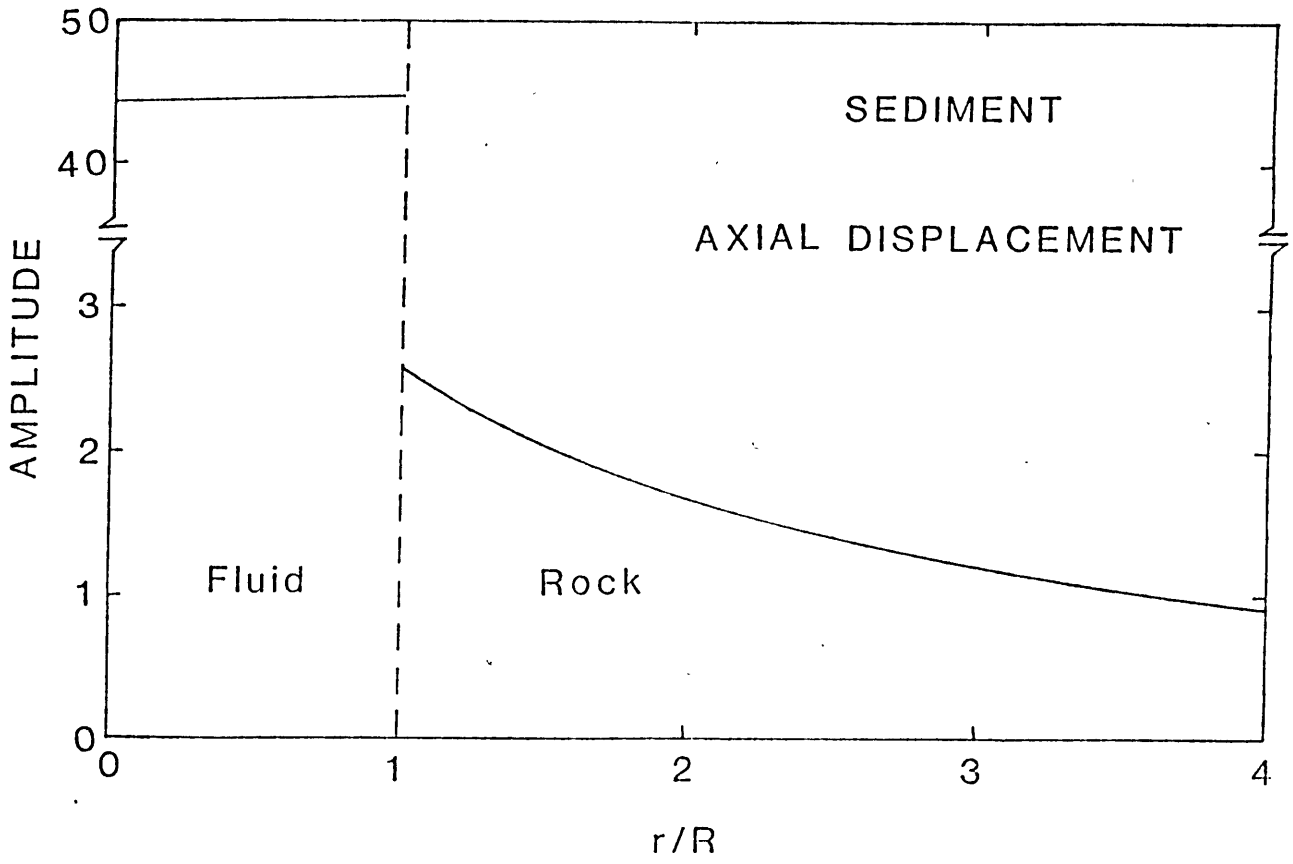

Figure 21.

(Cheng & Toksöz 1981)

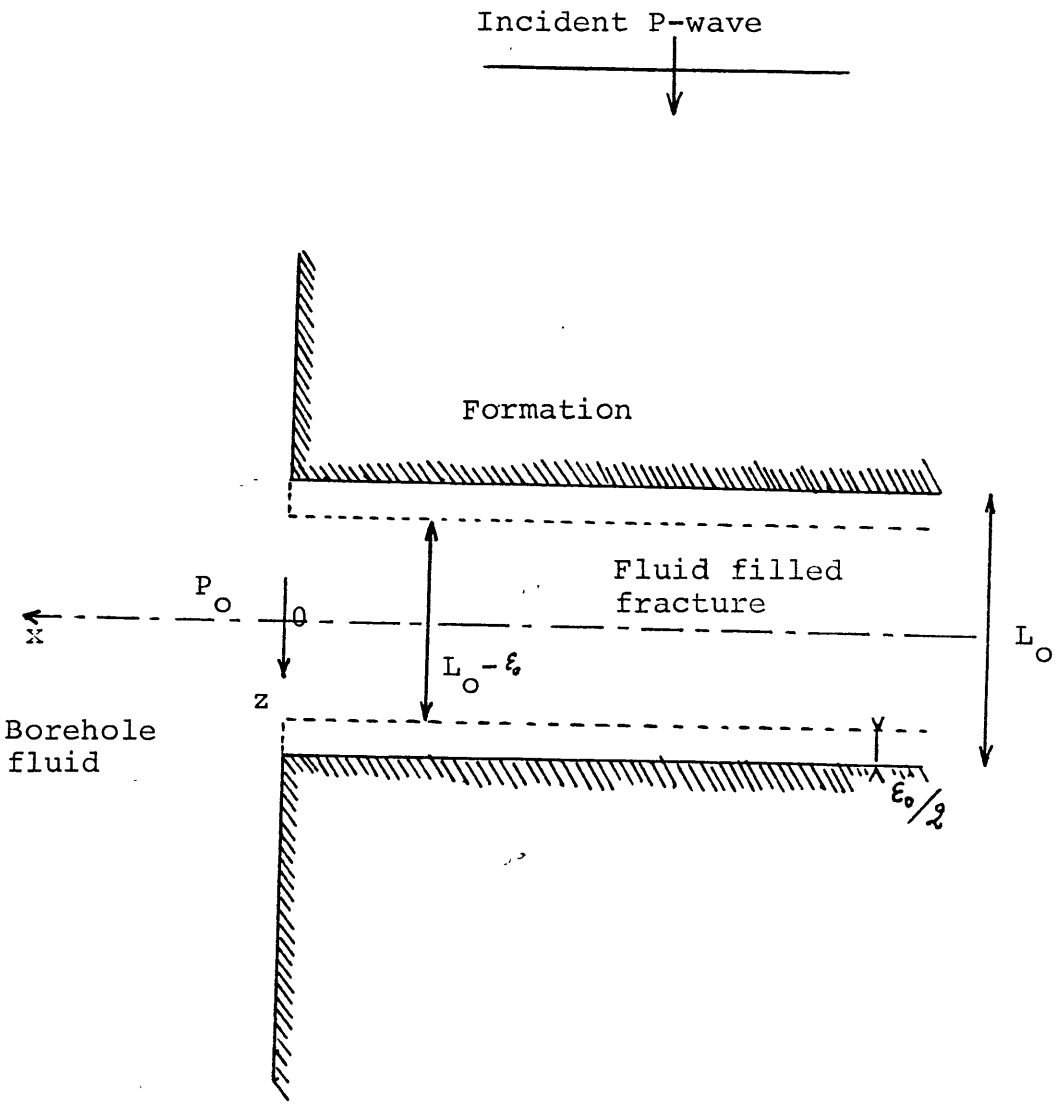
Incident P-wave
Formation
Fluid filled
fracture
P_o
0
x
z
$L_o - \varepsilon_o$
L_o
Borehole
fluid
y
$\varepsilon_o/2$

Figure 22.

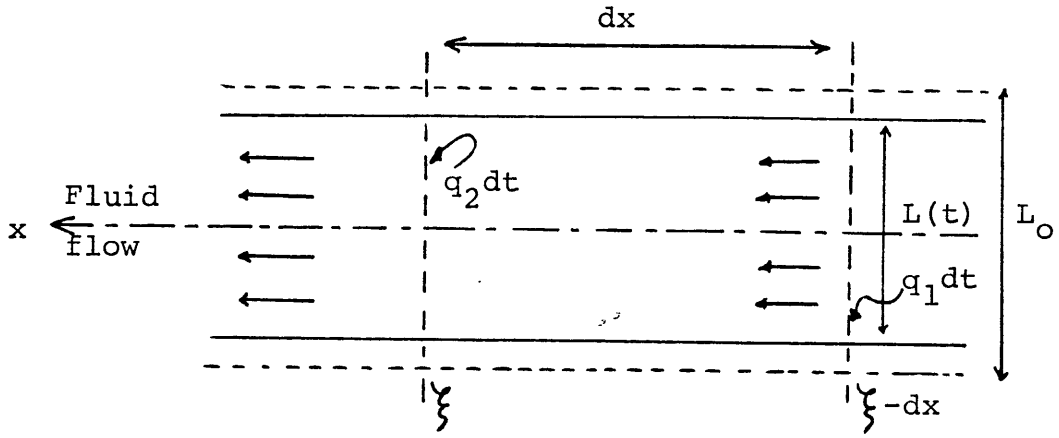

$$L(t) = L_o - \varepsilon_o \sin \omega t$$

Stored volume element $(q_1 - q_2)dt$

Figure 23.

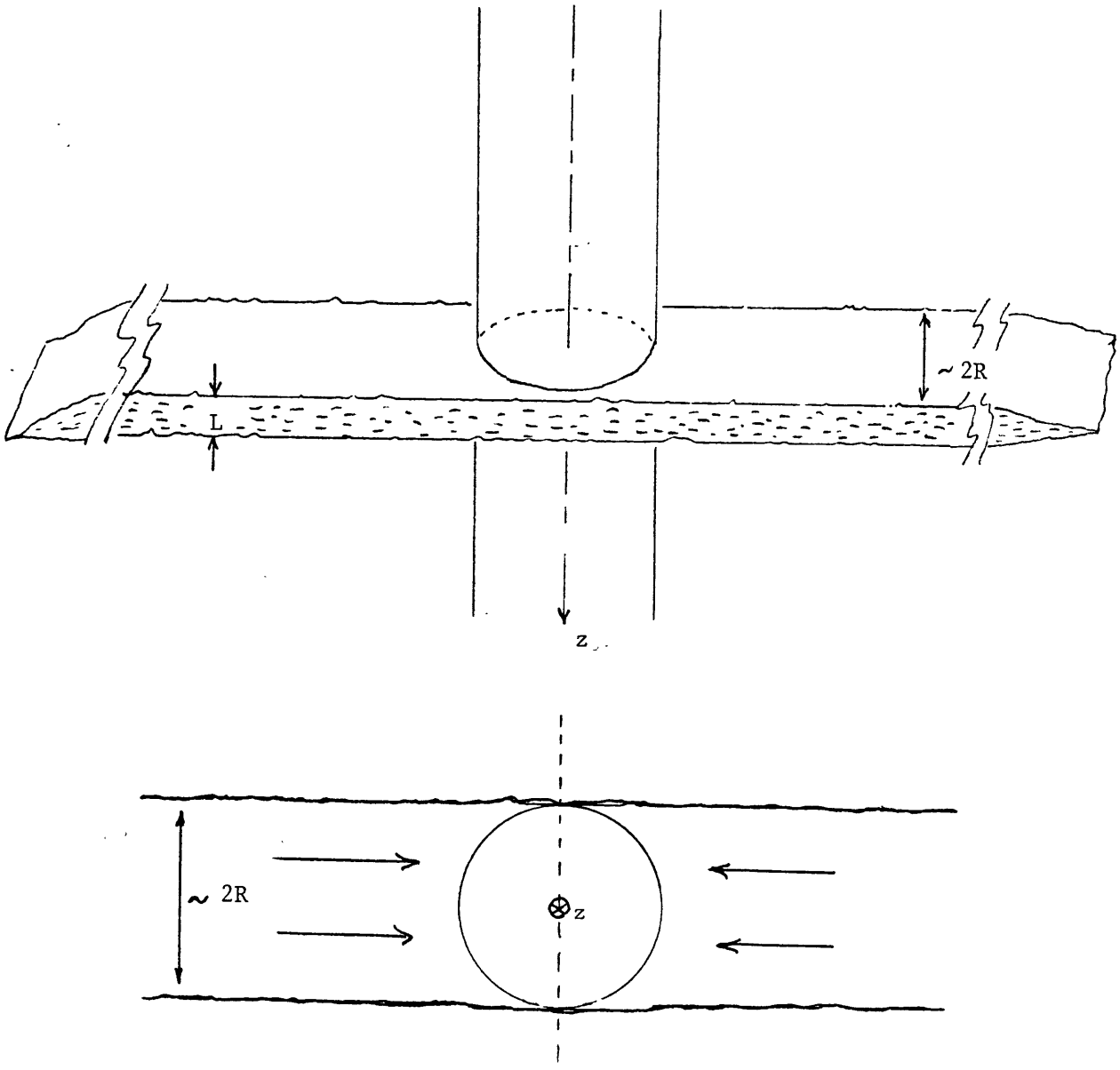

$$\Delta V_{3D} \sim 2 \times 2R \, \Delta V$$

Figure 24.

(Huang and Hunter 1981)

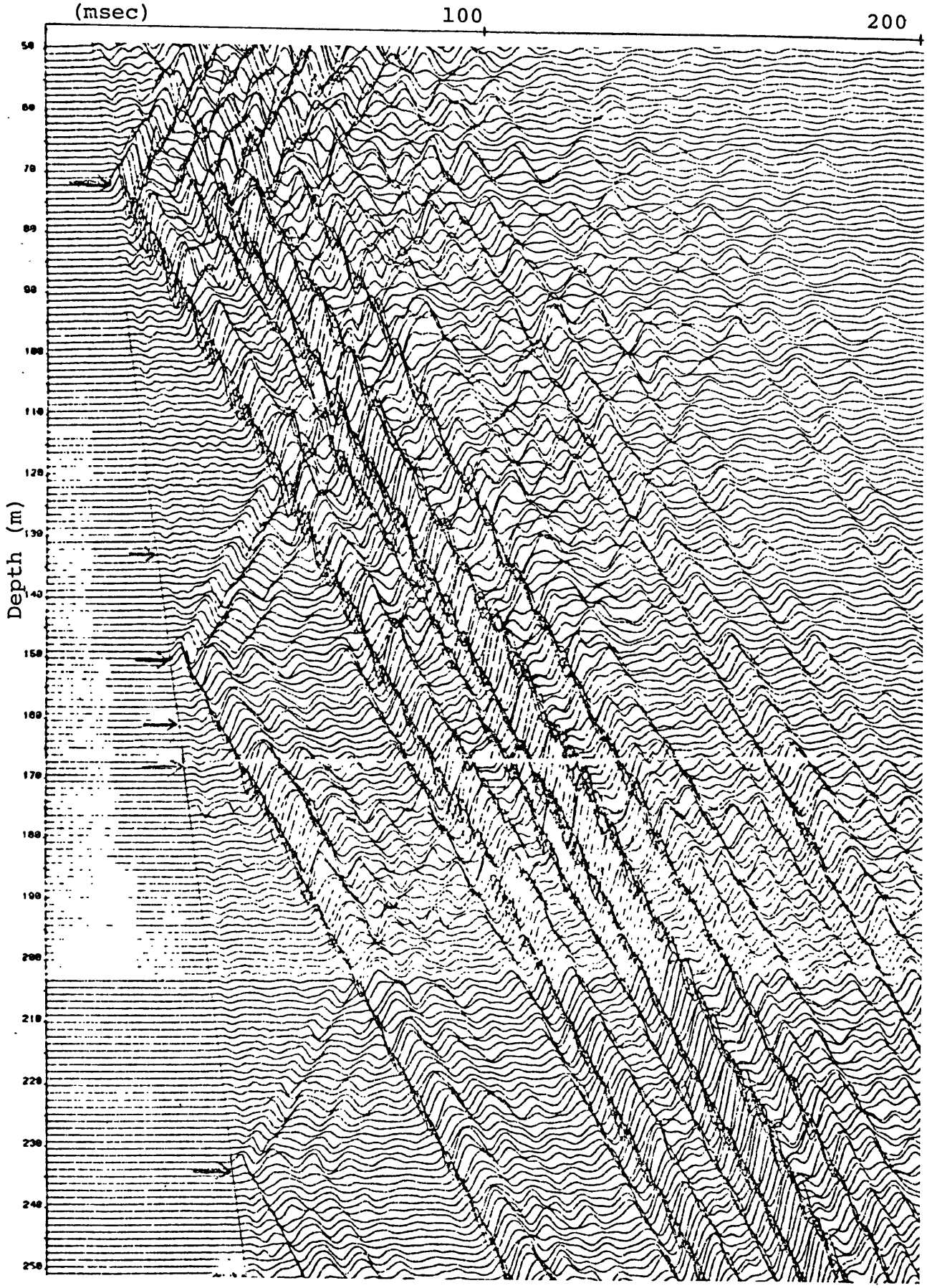

Figure 25.